



Cite this: *Phys. Chem. Chem. Phys.*,  
2018, 20, 23034

# Non-Gaussianity, population heterogeneity, and transient superdiffusion in the spreading dynamics of amoeboid cells†

Andrey G. Cherstvy,  \* Oliver Nagel, Carsten Beta and Ralf Metzler  \*

What is the underlying diffusion process governing the spreading dynamics and search strategies employed by amoeboid cells? Based on the statistical analysis of experimental single-cell tracking data of the two-dimensional motion of the *Dictyostelium discoideum* amoeboid cells, we quantify their diffusive behaviour based on a number of standard and complementary statistical indicators. We compute the ensemble- and time-averaged mean-squared displacements (MSDs) of the diffusing amoebae cells and observe a pronounced spread of short-time diffusion coefficients and anomalous MSD-scaling exponents for individual cells. The distribution functions of the cell displacements, the long-tailed distribution of instantaneous speeds, and the velocity autocorrelations are also computed. In particular, we observe a systematic superdiffusive short-time behaviour for the ensemble- and time-averaged MSDs of the amoeboid cells. Also, a clear anti-correlation of scaling exponents and generalised diffusivity values for different cells is detected. Most significantly, we demonstrate that the distribution function of the cell displacements has a strongly non-Gaussian shape and—using a rescaled spatio-temporal variable—the cell-displacement data collapse onto a universal master curve. The current analysis of single-cell motions can be implemented for quantifying diffusive behaviours in other living-matter systems, in particular, when effects of active transport, non-Gaussian displacements, and heterogeneity of the population are involved in the dynamics.

Received 5th July 2018,  
Accepted 8th August 2018

DOI: 10.1039/c8cp04254c

rsc.li/pccp

## 1. Introduction

### A. Diffusion of amoebae: biophysical properties

Complex active processes<sup>1–8</sup> are abundant in cell biology, ensuring motility and locomotion of cells,<sup>9–14</sup> swarming and chemotaxis of bacteria<sup>15–18</sup> and simple eukaryotes,<sup>19</sup> propulsion of natural or artificial micro-swimmers and microorganisms,<sup>1,17,20–31</sup> and diffusion of passive tracers in active bacterial suspensions.<sup>5,32</sup> Directed and collective motions<sup>10,33–37</sup> of eukaryotic cells on various substrates<sup>10,38,39</sup> are known to affect the features of embryonic development, wound healing, tumour migration<sup>40,41</sup> and cancer spreading.<sup>14,42–45</sup>

The social amoeba *Dictyostelium discoideum* (denoted as DICTY hereafter) is ubiquitously used as a eukaryotic model system to study cell motility,<sup>19,46</sup> aggregation and quorum sensing,<sup>47</sup> signal transduction, and cell-to-cell signalling.<sup>48,49</sup> In their natural habitats, free-living DICTY amoebae sense food

sources (bacteria) at a distance and pursue their prey *via* employing chemotactic mechanisms<sup>50–59</sup> and sensitively detecting chemoattractant gradients.<sup>54,56,60–64</sup> In particular, the vegetative-phase DICTY amoebae locate bacterial or yeast cells *via* folic-acid signals the latter secrete.<sup>50,57</sup> The dynamics of randomly-moving and chemotactic<sup>57,59</sup> DICTY cells were studied experimentally for different strains.<sup>19,46,51,53,65–68</sup> The reader is also referred to the computational studies of gradient sensing by chemotactic cells,<sup>69</sup> shape-driven cell migration,<sup>70</sup> and persistent pseudopodia formation.<sup>71</sup>

The spreading dynamics of DICTY cells (see Fig. 1a and b and the video files in the ESI†) involves the filopodia formation of (mainly) pseudopods.<sup>52,55,72</sup> Similarly to other motile cells,<sup>65,73</sup> DICTY actively creates rapid actin-rich pseudopodia protrusions on the leading edge (*via* actin polymerisation<sup>38</sup>) and retracts them on the back of the cell<sup>49,52,72,74–77</sup> with the help of myosin-II motors. This migration strategy is also employed by leukocytes and metastatic tumour cells.<sup>78</sup> A statistical analysis of pseudopod extension angles and centroid DICTY motions has been conducted.<sup>71</sup> The motion of pseudopodia is chemotactically-regulated directing cell migration.<sup>72</sup> The shape dynamics, wave propagation,<sup>52</sup> and migration of DICTY were considered,<sup>79</sup> see also ref. 47 for the DICTY social behaviour

Institute for Physics & Astronomy, University of Potsdam, 14476 Potsdam-Golm, Germany. E-mail: a.cherstvy@gmail.com, olnagel@uni-potsdam.de, beta@uni-potsdam.de, rmetzler@uni-potsdam.de

† Electronic supplementary information (ESI) available. See DOI: 10.1039/c8cp04254c

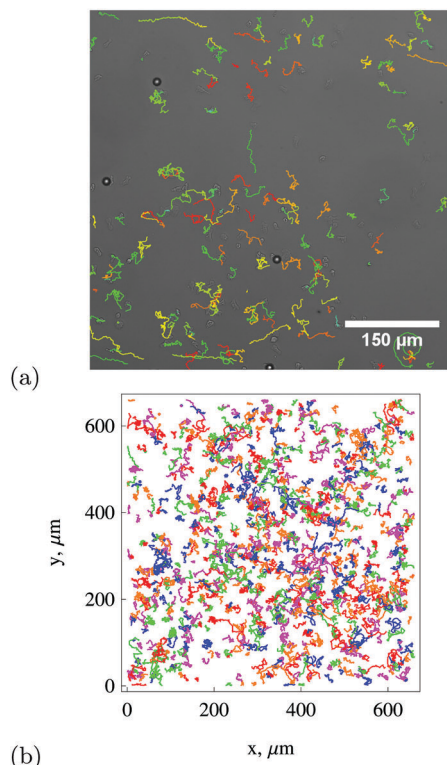


Fig. 1 Samples of experimentally recorded trajectories (at different starting times) (a) and all reconstructed traces of the DICTY cells (b) tracked in our experiments. Supporting video-microscopy files are provided in the ESI.†

and life cycle. Signalling pathways and cell-adhesion models of DICTY migration patterns were addressed as well.<sup>52,72,80</sup> In ref. 81 the details of recent atomic-force-microscopy measurements on amoebae–surface interactions are reported. When a starvation period begins, DICTY cells coordinate their motions, increase persistence and speed, and start forming actively-moving slug aggregates.<sup>46,47,56,64</sup>

For DICTY cells moving freely and without food sources on a two-dimensional agar surface at very low densities of  $\sim 1$  cell per  $\text{cm}^2$  (the AX4 strain) the directional persistence and turning angles were examined.<sup>19</sup> Importantly, the distribution of turning angles was found to be non-Gaussian, featuring an exponential tail. The time intervals between the directed DICTY turns were also found to be exponentially distributed.<sup>19</sup> Along the trajectories of individual amoebae, the clock- and counter-clockwise cell turning directions were shown to be anti-correlated.<sup>19</sup> The resulting zigzag motion of DICTY cells with long directional persistence may be favourable, *e.g.*, for optimising their food-search strategies<sup>58</sup> for sparse random targets.<sup>16,19,82–84,243</sup>

For other amoeboid cells (*e.g.*, for *Amoeba proteus*), the speed and turning angles were shown to be negatively correlated,<sup>86</sup> indicating that faster cells move more persistently, see Fig. 2 in ref. 47 and Fig. 3c in ref. 66. The universal features of cell migration based on actin-mediated flow patterns indicated pronounced correlations between the instantaneous speed and persistence time of motion for a number of different adherent cells,<sup>12,13</sup> including some amoebae. The measured speed distributions  $p(v)$  for planar

DICTY motion are roughly Maxwellian, but with fatter tails at large cell speeds<sup>19,66</sup> (as we also report below). The distribution of the components  $p(v_{x,y})$  was found to be non-Gaussian and to change drastically with the lag time.<sup>19</sup> This and other experimental evidence offer a field for an advanced statistical analysis and new theoretical approaches, beyond the standard models of passive diffusion.<sup>244</sup> In this paper, we report novel important insight into the properties of DICTY spreading/migration dynamics.

## B. Anomalous diffusion and physical description

The properties of the active motion of amoebae and of tracer particles<sup>87,88</sup> actively-driven in the highly-crowded DICTY cytoplasm<sup>89,90</sup> are examples of biological matter out of equilibrium.<sup>91,92</sup> Faster-than-Brownian dynamics is pertinent to active biological systems:<sup>20,93,94</sup> it is observed, *e.g.*, for swarming bacteria,<sup>16</sup> for the spreading of flagellate protozoa (transient superdiffusion),<sup>29</sup> and for the diffusion of some epithelial<sup>95</sup> and *Hydra* cells.<sup>26</sup> Note that superdiffusive Lévy walks can also describe collective motions of bacteria (with the outer region of expanding swarms of *Bacillus subtilis* obeying a persistent Lévy walk<sup>16</sup>) and motions of mRNA–protein complexes in a neuron.<sup>96</sup> We mention also correlated truncated Lévy processes proposed to rationalise diffusion in dilute suspensions of algae and bacteria.<sup>97</sup>

For non-Fickian diffusion, the standard measure of particle displacements—the ensemble-averaged mean-squared displacement (MSD)—grows anomalously with time in the power-law form,<sup>8,98–107</sup>

$$\text{MSD}(t) \simeq K_\alpha t^\alpha, \quad (1)$$

with the anomalous scaling exponent for superdiffusive motions being  $\alpha > 1$ . Here  $K_\alpha$  is the generalised diffusion coefficient. For passive subdiffusive tracer motions, abundant in viscoelastic and heterogenous biologically-relevant media,<sup>101,104,105,108–110</sup> one finds  $0 < \alpha < 1$ . The sublinear scaling of the ensemble- and time-averaged (a moving average defined in eqn (3) below) MSDs is fairly common for crowded cellular systems: for diffusion of lipids and proteins on two-dimensional membranes,<sup>111,112</sup> for obstructed viscoelastic motion of granules inside living cells,<sup>108,113,114</sup> and for motions of chromosomal loci in bacteria<sup>115–117</sup> and mammalian cells.<sup>118</sup> The cases  $\alpha = 1$  and  $\alpha = 2$  in eqn (1) describe Fickian/Brownian diffusion and ballistic motion, respectively.<sup>100,101</sup>

The diffusive motion of DICTY cells of different strains was thoroughly analysed.<sup>19,46,51,65,66</sup> For instance, it was shown<sup>66</sup> that the processes controlling DICTY speed and orientation involve a deterministic periodic component. Stretches of fast persistent motion were shown to be interrupted by slow phases, when reorientations of cell direction take place.<sup>66</sup> This intermittent DICTY kinetics is reminiscent of the alternating active–passive transport inside eukaryotic cells performed by dynein/kinesin motors<sup>3,93,94,119</sup> along microtubuli (see ref. 89 for transport inside DICTY and also ref. 87 and 120). An internal “clock” governs the cycles of DICTY motility and crawling, which include frequent shape deformations,<sup>73,79</sup> pseudopodia extension and retraction,<sup>66,71,121</sup> and formation of actin polymerisation waves.<sup>121–123</sup> Also, the “turning rate” and the speed of DICTY persistent motion are anti-correlated<sup>66</sup> (also ref. 46, but contrast to Fig. 2 of ref. 47).

The amoebae diffusion can be viewed as directed motions with intermittent directional turnings of the cells.<sup>66</sup>

A number of theoretical models have been proposed to describe the dynamics of actively-driven tracers and bacteria, with different noise terms employed to describe azimuthal motions and axial propulsions, see a recent review.<sup>20</sup> Some physical models of active tracers<sup>14,19,20,124–134</sup> were applied to cell crawling, also for amoebae (see the recent study<sup>73</sup> of crawling and cell-shape dynamics of the fibroblast cells). Physically, for active two-dimensional motions of an elongated particle at short times a persistent motion is expected. For times much longer than the typical persistence time of directed motions,  $t \gg t_p$ , multiple azimuthal turnings occur and the transition to Fickian diffusion takes place for the center of mass of the particles. Note that the short-time DICTY diffusivities are broadly distributed,<sup>19</sup> indicating a cell-to-cell variability (fast, intermediate, and slow cells exist in a population<sup>47</sup>). Finally, the Monte Carlo simulations<sup>19</sup> for a coloured noise-driven orientational “DICTY-particle” have reproduced the exponential distribution of the turning angles and other features of amoeboid superdiffusion.

Still, some important details of the DICTY dynamics remain to be quantified, which is our main focus here using detailed statistical analysis. We quantify the ensemble- and time-averaged MSDs, and also report the distribution of scaling exponents and diffusivities of individual DICTY cells. Moreover, we compute and rationalise the evolution of non-Gaussian distributions of DICTY displacements and unveil the universal features of amoeba spreading dynamics, which are consistent with the anomalous MSD law we observe. These central novel results of our combined experimental and data-analysis study will also be relevant for the spreading dynamics of other self-propelled cells.

## II. Results of statistical data analysis

We perform a model-free analysis of the experimentally-recorded DICTY traces, see Fig. 1, based on multiple statistical indicators. We compute the ensemble- and time-averaged MSDs, the spread and correlation of anomalous scaling exponents *versus* respective instantaneous diffusion coefficients, the distribution of cell displacements and speeds, and the velocity–velocity autocorrelation function.

### A. Ensemble and time-averaged MSDs

The recorded single-cell trajectories for  $N \approx 1100$  tracked DICTY cells are presented in Fig. 1b. The trace length  $T$  is broadly distributed,  $T \approx 60 \dots 940$  time steps, due to experimental limitations, see Section IV. One step (denoted  $s$  below) corresponds to  $\delta t = 20$  s, so that the total DICTY tracking time is  $\sim 0.3 \dots 5$  hours, see Fig. 9. Based on the displacement data for DICTY cells, we calculate both the ensemble- and time-averaged MSDs, and compare their behaviour in Fig. 2. A two-parameter fit of the short-time MSD growth shows that it is anomalous,

$$\text{MSD}(t) = \langle [x(t) - x(0)]^2 + [y(t) - y(0)]^2 \rangle \sim K_\alpha t^\alpha, \quad (2)$$

with the superdiffusive scaling exponent  $\alpha \approx 1.28$ . Note that a random component of the DICTY motion may stem from internal noisy processes and as a response to medium inhomogeneities.<sup>51</sup> The individual time-averaged MSD trajectories, evaluated from displacements of the centre of mass of the  $i$ th DICTY cell as<sup>100,101,103,113</sup>

$$\overline{\delta^2(\Delta)} = \frac{\int_0^{T-\Delta} \{ [x_i(t+\Delta) - x_i(t)]^2 + [y_i(t+\Delta) - y_i(t)]^2 \} dt}{T - \Delta}, \quad (3)$$

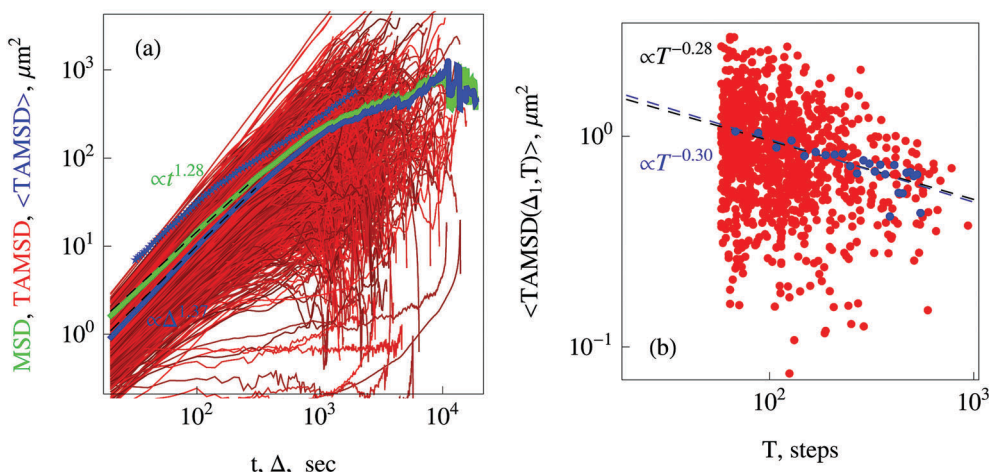


**Fig. 2** Panel (a): ensemble- and time-averaged MSDs plotted *versus* (lag) time  $t, \Delta$ . The MSD and mean time-averaged MSD are the solid green and blue curves, respectively. Individual  $\overline{\delta^2(\Delta)}$  traces are the red lines, while the red dots in panel (b) are the initial values  $\overline{\delta^2(\Delta_1)}$  at  $\Delta_1 = 20$  s. The asymptotes of eqn (1) and (7) with  $\alpha \approx 1.28$  and  $\beta \approx 1.37$  for the ensemble-averaged and mean time-averaged MSDs are the dashed black lines, respectively. For comparison, in panel (a) we show as the blue stars the mean time-averaged MSD data from Fig. 1E of ref. 47 (for the DH1 DICTY strain). Panel (b): Scatter of initial time-averaged MSD values  $\overline{\delta^2(\Delta_1)}$  and their dependence on the trace length  $T$ , see eqn (7). The direct fit of  $\overline{\delta^2(\Delta_1, T)}$  data as a power-law function of  $T$  is the black dashed line. The results of averaging over first equidistantly-binned  $\overline{\delta^2(\Delta_1, T)}$  data (the blue dots) is the dashed blue line. The density of points in panel (b) reflects the  $p(T)$  histogram of Fig. 9, with  $T_{\min} = 60$  steps being the minimal length of the analysed cell trajectories.

reveal a pronounced spread of magnitudes and scaling exponents, even for lag times much shorter than the trace length,  $\Delta \ll T$ , see Fig. 2. Such trajectory-to-trajectory variations emerge here, *i.e.*, due to inherent variations in physical dimensions of cells and different propulsive characteristics in the cell population, as well as variations of the actual age of a given cell being tracked. Such variations of the time-averaged MSD are also quite typical for non-ergodic anomalous diffusion processes taking place at, for instance, heterogeneous conditions across the system, see ref. 101 and 136–139 and also the discussion in Section III. The spread of magnitudes and scaling exponents for individual time-averaged MSD trajectories with the scaling

$$\overline{\delta_r^2(\Delta)} \simeq K_{\beta,i} \Delta^{\beta_i} \quad (4)$$

also grows for progressively larger lag time values  $\Delta$ . That is a rather standard feature for various stochastic processes,<sup>100,101,114</sup> including standard Brownian motion (due to the decreasing sample size for fixed  $T$ ). Hereafter, the overline denotes time averaging and the angular brackets indicate ensemble averaging. We define the mean time-averaged MSD as the average over  $N$  trajectories,

$$\langle \overline{\delta^2(\Delta)} \rangle = N^{-1} \sum_{i=1}^N \overline{\delta_r^2(\Delta)}. \quad (5)$$

As compared to the ensemble average (1), at short lag times  $\Delta$  the mean time-averaged MSD  $\langle \overline{\delta^2(\Delta)} \rangle$  for the DICTY data set grows with a slightly different exponent,  $\beta \approx 1.37$ . The reported exponents  $\alpha$  and  $\beta_i$  are obtained here *via* two-parameter fits of the first  $n_{\text{fit}} = 15$  points of the cell traces (using Wolfram Mathematica). These rather small numbers of fitting points describe the initial growth of individual time-averaged MSD trajectories at short lag times, *i.e.*, in the regime where the mathematical description by moving averages is statistically most reliable. Provided a limited total number of points in an average track recorded, these fitting numbers seems realistic to capture the short-time growth of the MSD. We refer the reader to ref. 135 for effects of the number of lag-time fitting points on the estimation of scaling exponents.

In Fig. 2a the MSD and mean time-averaged MSD are fairly close, but do not match perfectly, both in terms of their amplitudes and scaling exponents. This discrepancy between the ensemble- and time-averaged particle displacements signifies the phenomenon of so-called weak ergodicity breaking, see ref. 8, 100, 101, 103, 136, 137 and 141–144. Note, however, that this relatively minor discrepancy may be diminished further when more and longer traces are used in the analysis, also provided *via* different data-acquisition strategies. In Fig. 2a we additionally present the ensemble- and time-averaged MSDs for the DH1 DICTY strain, for comparison with our findings. As the diffusive dynamics of DICTY cells is known to depend strongly on their strain or cell-line,<sup>46</sup> the sample preparation procedure, surface properties, some ageing effects,<sup>47</sup> *etc.*, the discrepancy with ref. 47 in terms of the MSD magnitude and scaling exponent we observe is not that surprising.

The distribution of time-averaged MSDs of DICTY cells is shown in Fig. 3 for varying lag-time values. Corroborating the

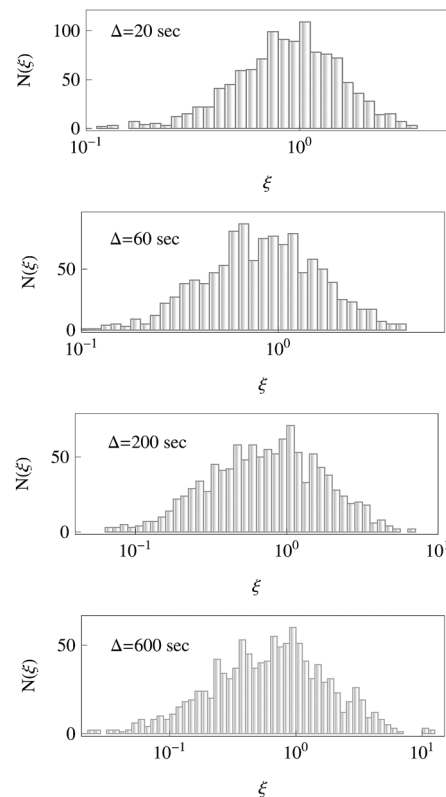


Fig. 3 Amplitude scatter of time-averaged MSDs in terms of number distributions  $N(\xi = \overline{\delta^2(\Delta)} / \langle \overline{\delta^2(\Delta)} \rangle)$  for the data set of Fig. 2, plotted for lag times  $\Delta = \{20, 60, 200, 600\}$  s. Very small  $\overline{\delta^2}$  magnitudes (nearly immobile cells) are not shown.

results of Fig. 2a, we find that the scatter of  $\overline{\delta^2}$  magnitudes is growing with the lag time.

The moderate transient superdiffusion we find for the AX2 DICTY strain differs from the findings of ref. 19 for the AX3 strain at similarly low cell densities. Namely, for the AX3 strain at short times the time-averaged MSD grows roughly ballistically, while diffusion turns Brownian at longer times,  $t \gtrsim 20$  min. The model of persistent two-dimensional random walks—with a characteristic velocity  $v_p \approx 5.4 \mu\text{m min}^{-1}$  and persistence time  $t_p \approx 8.8$  min—was shown to fit the data,<sup>19</sup> namely

$$\langle \overline{\delta_{\text{WLC}}^2(\Delta)} \rangle = 2v_p^2 t_p^2 \left[ \Delta/t_p - \left(1 - e^{-\Delta/t_p}\right) \right]. \quad (6)$$

Here the subscript WLC refers to the worm-like-chain model. The same functional form but with  $t_p \sim 5$  min was used to describe diffusion for the DH1 strain,<sup>47</sup> as well as in the classical study<sup>46</sup> for the NC4 strain. In ref. 46 significant correlations of diffusion coefficients,  $D = K_1 = v_p^2 t_p/2$ , with mean cell velocities were documented, in addition to inverse correlations of  $t_p$  with  $v_p$ .<sup>245</sup>

## B. Effects of trace-to-trace variability and the cell trajectory length

As Fig. 2a illustrates, the scaling exponents of the ensemble- and time-averaged MSDs are progressively decreasing with the

(lag) time. Towards the end of the trajectories, a much slower growth of cell displacements is detected, with  $\alpha \approx \beta \approx 0.3$ , a feature of confined or ageing subdiffusion<sup>100,101,137</sup> that may, however, be caused by the current data-acquisition protocol (with its intrinsic limitations) as well as by cell sample-preparation methods, see Section IV for details. The fastest DICTY cells quickly leave the field of observation (in the vertical direction; see also Fig. 2 in ref. 16), possibly contributing to this MSD slowing-down at later stages. Because of this experimental limitation, longer trajectories in the data set may contain a *bias* towards slower cells. Their subpopulation will be over-represented in such an ensemble, thereby giving rise to overall smaller magnitudes for cell displacements. A similar bias towards slower walkers can emerge for longer minimal trace lengths,  $T_{\min}$ , that are set at the start of the tracking experiment, see the discussion in ref. 145, 147 and 155. Note that for spreading of protozoa a similar dramatic reduction of the local scaling exponent along the traces was detected, see Fig. 2b of ref. 29 and 246–248.

As the trace length  $T$  varies among the trajectories, see Fig. 9, in Fig. 2b we quantify the dependence of the initial time-averaged MSD value at the first time-step  $\overline{\delta^2(\Delta_1 = 1)}$  on  $T$ . We find that shorter trajectories yield slightly but systematically larger  $\overline{\delta^2(\Delta_1)}$  values and a more pronounced spread, see Fig. 2b. The  $\overline{\delta^2(\Delta_1)}$  magnitudes decrease on average with  $T$ , possibly due to some tracking-method-related bias towards monitoring a subpopulation of slower cells for longer  $T$ . Note that one expects an opposite behaviour of  $\overline{\delta^2(\Delta_1, T)}$  versus  $T$  for a free superdiffusive process. Some *inherent ageing* effects—known to occur for DICTY motion<sup>46,47,148</sup>—and the above-mentioned escape of faster cells from the view-field may also contribute to the decrease of  $\overline{\delta^2(\Delta_1, T)}$  with  $T$  reported in Fig. 2b.

Fitting this dependence with a simple power law, the short-lag-time diffusion law consistent with the data is

$$\langle \overline{\delta^2(\Delta, T)} \rangle \simeq \langle K_{\beta_i} \Delta^{\beta_i} \rangle / T^{\alpha-1}, \quad (7)$$

with broadly-spread generalised diffusion coefficients,  $K_{\beta}$ . Fitting the data of Fig. 2b gives  $\alpha \approx 1.28 \dots 1.3$ , consistent with the MSD exponent of Fig. 2a and the spreading law (7). Moreover, the exponent of the decay of  $\langle \overline{\delta^2(\Delta_1, T)} \rangle$  with  $T$  stays nearly unaltered if we first order the  $\overline{\delta^2(\Delta_1)}$  values into equidistant  $T$ -bins and then fit the data, see the black and blue dashed lines in Fig. 2b.

The initial growth of the ensemble- and time-averaged MSDs with (lag) time and their magnitudes provide an estimate of the short-time diffusivity of the AX2 DICTY strain, namely  $\langle D \rangle \sim 0.03 \mu\text{m}^2 \text{s}^{-1} = 1.8 \mu\text{m}^2 \text{min}^{-1}$  (note that cell motion is initially slightly superdiffusive). This is considerably smaller than for a slower subset in a DICTY DH1 population reported in ref. 47, where  $\langle D \rangle \approx 4.7 \mu\text{m}^2 \text{min}^{-1}$ . This discrepancy is reflected in the MSD magnitude; compare the blue curve and blue data points in Fig. 2a.

### C. Generalised diffusion coefficients and anomalous scaling exponents: anti-correlations

Fig. 1 and 2 illustrate strongly heterogeneous features of amoebae diffusion. Specifically, some DICTY cells move in a rather persistent manner, while others perform a fairly confined motion. These two distinct types of motion result in, respectively, fast superdiffusively growing and nearly stalling  $\overline{\delta^2(\Delta)}$  traces, Fig. 2a. Moreover, the distributions of scaling exponents  $p(\beta)$  and generalised diffusion coefficients  $p(K_{\beta})$  are also significant. We quantify  $p(\beta_i)$  in Fig. 10 *via* power-law fitting of initial  $n_{\text{fit}} = \{5, 15, 25\}$  points of  $\overline{\delta^2(\Delta)}$  trajectories.

We observe that the  $p(\beta)$  shape is somewhat asymmetric, with the largest exponents  $\beta \approx 2$  for nearly ballistic motion of highly-motile cells. The error bars for extracted scaling exponents get smaller when more points are used in the fitting analysis. The initially stalling traces in Fig. 2a are the entries with  $\beta \approx 0$  in Fig. 10. We find that a smaller number of fit points  $n_{\text{fit}}$  at short lag times  $\Delta/T \ll 1$  gives larger exponents  $\beta$ , compare the panels of Fig. 10; the DICTY motion we detect becomes less persistent with time, turning from superdiffusion into subdiffusion with increasing lag time  $\Delta$ . The  $p(\beta)$  distributions provide well-defined mean values,  $\langle \beta \rangle$ , which also shift by a similar margin  $\delta \langle \beta \rangle \approx 0.1$  when the  $\overline{\delta^2(\Delta)}$  traces from Fig. 2 are fitted using smaller  $n_{\text{fit}}$  values.

Naturally, the fitting procedure (4) depends on the number of fitting points  $n_{\text{fit}}$  and on data binning (linear, log, *etc.*), making the results for  $K_{\beta}$  and  $\beta$  somewhat non-universal. We refer here to the recent studies on optimisation methods for evaluation of diffusion coefficients and anomalous scaling exponents for  $\overline{\delta^2(\Delta)}$  from single-particle tracking data,<sup>149–151</sup> also in the presence of particle-localisation errors.<sup>152</sup>

The distribution of the short-lag-time generalised diffusion coefficients,  $p(K_{\beta})$ , is shown in Fig. 11. For smaller  $n_{\text{fit}}$  values the shapes of  $p(K_{\beta}/\langle K_{\beta} \rangle)$  appear more peaked or localised. Moreover, the “averaged” generalised diffusion coefficient increases with the number of fitting points: for  $n_{\text{fit}} = \{5, 15, 25\}$  we find, respectively,  $\langle K_{\beta} \rangle \approx \{0.020, 0.043, 0.100\} \mu\text{m}^2 \text{per s}^{(\beta)}$ , with scaling exponents  $\langle \beta \rangle \approx \{1.37, 1.25, 1.15\}$ , see Fig. 4, 10 and 11. Note that we compare here generalised diffusion coefficients seemingly having different units; one can “regularise” this inconsistency if  $K_{\beta,i}$  values are multiplied by the unit lag time to the corresponding power  $\beta_i$ , eqn (4). Then, the corresponding spread of time-averaged displacements will be effectively compared (as, for instance, in Fig. 7 of ref. 153); see also recent studies<sup>155,156</sup> as examples of quantifying the spread of generalised diffusion coefficients directly. The mean values of generalised diffusion coefficients and scaling exponents are given here in the sense of ensemble averages, eqn (7).

The pronounced  $K_{\beta}$ -spread we find is consistent with (some) previous findings (see, *e.g.*, Fig. 3A of ref. 19). We also refer to ref. 157 for quantifying the effects of statistical and instrumental spreading of diffusion coefficients *via* simulations. The spread of generalised diffusion coefficients and scaling exponents (see also ref. 75)—that stems, *i.a.*, from different DICTY shapes, sizes, and propulsion strategies—contributes to variable migration and fitness properties of amoeboid cells.<sup>46</sup>

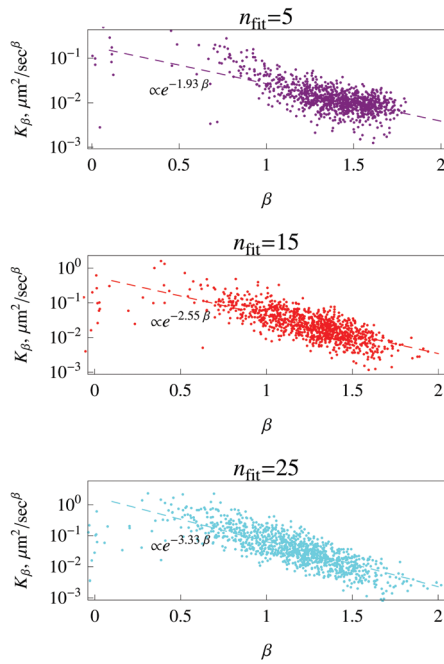


Fig. 4 Anticorrelation of scaling exponents and generalised diffusion coefficients for the data of Fig. 2. The best-fit asymptotes (8) are the dashed lines. The colours for  $n_{\text{fit}} = \{5, 15, 25\}$  initial fitting points of the  $\overline{\delta^2(A)}$  are purple, red, and cyan, respectively (for these plots as well as for Fig. 10 and 11).

Moreover, we detect pronounced anti-correlations of  $\beta$  versus  $K_\beta$ , with the Pearson correlation coefficient for the  $\{K_\beta, \beta\}_{n_{\text{fit}}}$  sets being  $\approx \{-0.56, -0.50, -0.51\}$  for  $n_{\text{fit}} = \{5, 15, 25\}$ , respectively. The DICTY cells diffusing more persistently exhibit (on average) smaller diffusivities. To quantify this important feature of the dynamics, we show in Fig. 4 the  $K_\beta(\beta)$  data on a log-linear scale, together with the two-parameter fitted exponential slopes

$$K_\beta(\beta) \sim \exp[-c_1\beta + c_2]. \quad (8)$$

To the best of our knowledge, none of the standard anomalous diffusion processes<sup>100,101</sup> features such anti-correlations, challenging the physical explanation and mathematical description of the observed amoebae dynamics. For instance, for viscoelastic diffusion of tracers in polymeric hydrogels<sup>146,147</sup>  $K_\beta$  versus  $\beta$  correlations are positive.<sup>158</sup> A simplistic view of these remarkable  $K_\beta$  versus  $\beta$  anti-correlations is that some cells use the energy sources available so that more persistent active motions at lower diffusivities are realised, while other cells diffuse in a more random manner (less persistently), but instead with larger diffusivities. These intrinsic heterogeneities in the *in vitro* population of the DICTY cells may have implications, *i.e.*, for optimising the food-search strategies<sup>19,58</sup> they employ *in vivo*.

#### D. Non-Gaussian displacement distributions

We examine the probability distribution functions of DICTY displacements focusing on their pronounced non-Gaussian features. The universal space-time rescaled distribution function  $p(z \approx \delta x/(\delta t)^{0.615})$  found below is our central novel

result here. The distributions of displacements  $p(\delta x)$  for all cells in the data set along the coordinate  $x$  for the chosen time-shifts of

$$\delta s = 1, 3, 10, \text{ and } 30 \text{ steps} \quad (9)$$

are shown in Fig. 5 on a log-linear scale ( $\delta t = \delta s \times 20$  s). The distributions along the  $y$ -direction,  $p(\delta y)$ , reveal nearly identical non-Gaussian features, as confirmed in Fig. 12. We focus below on the shapes of  $p(\delta x)$ , which reveal pronounced cusps at  $\delta x = 0$  for all  $\delta s$  values (9), see Fig. 13, a very distinct feature as compared to the standard Gaussian. The decay of the tails of  $p(\delta x) \propto N(\delta x)$  distributions is slower than Gaussian (here,  $N(\delta x)$  is the number of cell displacements for given  $\delta x$  and  $\delta t$  values in the data set).

We find that the exponent  $\delta$ —quantifying the decay of  $p(\delta x)$  away from the cusp—is fairly close to unity, resulting in a Laplace-like exponential (rather than in a Gaussian) distribution. The exponent decreases slightly with  $\delta t$  so that the distribution becomes roughly exponential at longer time-shifts, see Fig. 5 and 12. The decrease of exponent  $\delta$  with step-shift  $\delta s$  we find is not surprising: as Fig. 2 illustrates, for longer lag times  $A$  the dynamics of DICTY cells slows down in terms of the exponent  $\langle\beta(A)\rangle$ . To quantify these features, we fit the reconstructed distributions  $p(\delta x)$  using Wolfram Mathematica with a two-parametric zero-mean compressed exponential or stretched Gaussian distribution,

$$p_{\delta,\sigma}(\delta x) \approx \frac{1}{2\sigma^2\delta^{1/\delta}\Gamma(1+1/\delta)} \exp\left[-\frac{1}{\delta}\left(\frac{|\delta x|}{\sigma}\right)^\delta\right], \quad (10)$$

where  $\sigma$  is the characteristic width of the distribution and  $\Gamma(x)$  is the Gamma function. The notation  $\delta$  for the exponent in (10) (following ref. 106) should not be mixed with  $\overline{\delta^2(A)}$  and space or time increments,  $\delta x$  or  $\delta t$ . The averaged squared cell displacements along the  $x$ -direction,  $\langle(\delta x)^2\rangle$ , then scale with the time-shift  $\delta t$  as

$$\begin{aligned} \langle(\delta x)^2(\delta t)\rangle &= 2 \int_0^\infty (\delta x)^2 p_{\delta,\sigma}(\delta x) d(\delta x) \\ &= \frac{\sigma^2(\delta t)\langle\delta\rangle^{2/(\delta)}\Gamma(3/\langle\delta\rangle)}{\Gamma(1/\langle\delta\rangle)} \sim \sigma^2(\delta t). \end{aligned} \quad (11)$$

Here, we neglected a weak dependence of the exponent  $\delta$  on the time-shift (see Fig. 5 and 12), using in further analysis the average  $\langle\delta\rangle$  value over all the time steps  $\delta t$  examined. This provides a good description of the displacement data, see Fig. 7 and 14.

From the best-fit parameters of the distribution functions of Fig. 5, 12 and 13, we find that the width of the distribution grows with  $\delta t$  in a non-Fickian manner,

$$\sigma(\delta t) \sim (\delta t)^{0.615}, \quad (12)$$

identical for  $x$ - and  $y$ -displacements, as shown in Fig. 6. Thus, introducing the rescaled space-time variable

$$z = (\delta x)/(\delta t)^{0.615} \approx (\delta x)/(\delta t)^{2/3}, \quad (13)$$

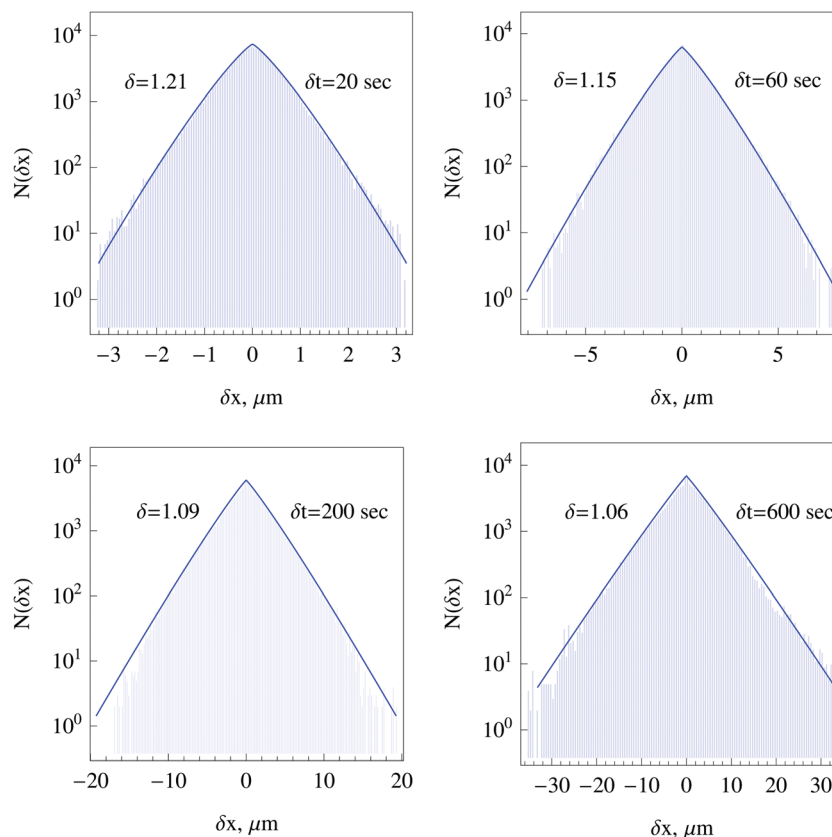


Fig. 5 Log-linear histograms of the number of cell displacements along the x direction for different time-shifts  $\delta t$ , as indicated in the plots. Different horizontal scales in the panels are to be noted. The asymptotes of eqn (10) are the blue curves, with the values of the best-fit exponent  $\delta$  provided in each panel.

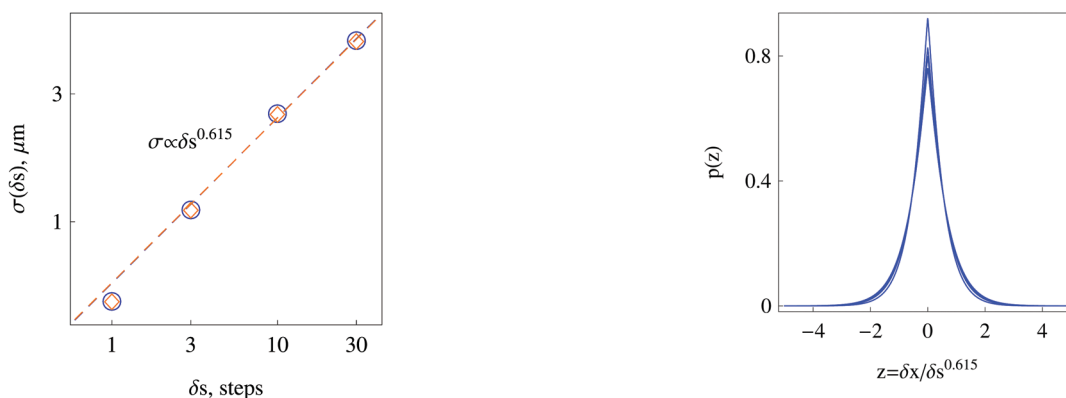


Fig. 6 Width of the distributions  $\sigma(\delta s)$  versus time-shift, as found via the best fit of  $p(\delta x)$  and  $p(\delta y)$  of Fig. 5 and 12. The circles and diamonds are the data for the x and y direction, respectively. The power law (12) is the dashed line ( $dt = ds \times 20$  s).

the rescaled displacement distributions for different time-shifts should collapse onto the universal master curve, see Fig. 7 and 14, namely

$$p_{\delta, \sigma(\delta t)}(\delta x) \sim \exp\left(-\left[\frac{\delta x}{(\delta t)^{0.615}}\right]^\delta\right). \quad (14)$$

Similar dependencies were recently detected also, *e.g.*, in ref. 111 and 159, see also Appendix B. The standard Gaussian for normal diffusion follows from eqn (10) for  $\alpha = 1$  and  $\delta = 2$ .

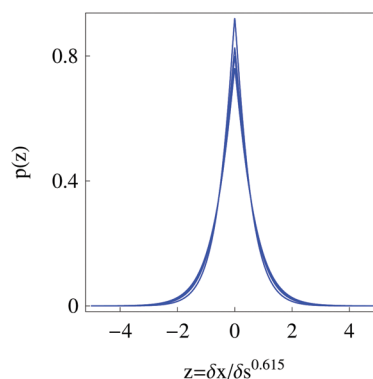


Fig. 7 Collapse of probability distributions in terms of the rescaled variable  $z$ , given by eqn (13), plotted for the time-shifts and mean scaling exponent ( $\delta$ ) from the data of Fig. 5.

Using eqn (12) and (13) we find that the superdiffusive exponent is  $\alpha \approx 2 \times 0.615$ , which is close to  $\alpha \approx 1.28$  obtained from the short-time MSD growth in Fig. 2a, in accordance with eqn (11). The logarithmic and linear histograms of Fig. 5 and 13 demonstrate that eqn (10) and (14) describe the DICTY cell displacement data very well.

The DICTY cells thus have pronouncedly non-Gaussian displacement distributions and diffuse anomalously. Therefore, the currently-investigated Brownian but non-Gaussian

“diffusing diffusivity” models<sup>159–166</sup> should be modified to become appropriate to describe these observations (see, *e.g.*, ref. 164, 166 and the discussion in Section III below). Generally, superstatistical approaches<sup>167</sup> may be appropriate here due to the observed heterogeneity in the DICTY dynamics on the population level.

### E. Speed distribution and velocity–velocity auto-correlation function

The instantaneous speed of a given cell at time-step  $i$ , is defined as the ratio of displacement increments over the elementary (finite) time step in the experiments,

$$v_i = \sqrt{(x_{i+1} - x_i)^2 + (y_{i+1} - y_i)^2} / dt. \quad (15)$$

This quantity fluctuates broadly along the recorded DICTY trajectories (not shown). Theoretically, the shape of the  $p(v)$  distribution delivers important information regarding the type of underlying active dynamics.<sup>20,131</sup> The profile of DICTY speeds  $p(v)$  in Fig. 8—obtained after averaging over all cells and time steps—cannot be satisfactorily fitted *via* the one-parameter Rayleigh-like distribution

$$p_{\text{Ray}}(v) = \frac{v \exp[-v^2 / (2\sigma_v^2)]}{\sigma_v^2}. \quad (16)$$

This would correspond to the Maxwell–Boltzmann profile expected for an equilibrium system with average squared particle speed  $\langle v^2 \rangle = 2\sigma_v^2 = 2k_B T_{\text{eff}} / m$ , where  $T_{\text{eff}}$  is the effective temperature and  $m$  is the particle mass, see also ref. 5 and 32. The measured DICTY  $p(v)$  function grows faster at small speeds and has more pronounced tails at high speeds, see Fig. 8. The latter were indeed observed in the earlier examinations of the DICTY motility (see Fig. 2 and 5 of ref. 46 and Fig. 6 of ref. 66).

Fitting our data with the two-parameter generalised Gamma distribution

$$p_{\text{Gam}}(v) = \frac{\gamma v^{\gamma-1} \exp[-v^\gamma]}{\Gamma(\gamma)} \quad (17)$$

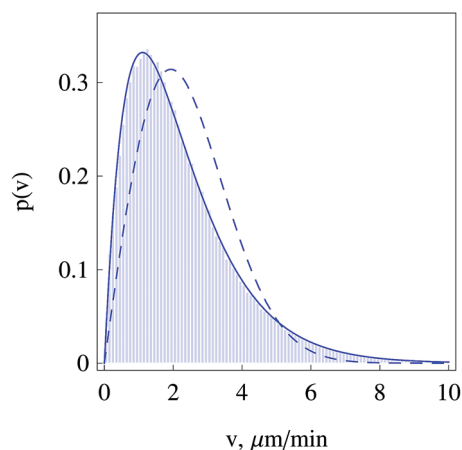


Fig. 8 Distribution of instantaneous cell speeds  $p(v)$  and its fit by the Rayleigh (16) and generalised Gamma (17) distributions (the dashed and solid curves, respectively).

provides a much better agreement. The fit function shown in Fig. 8 is  $p_{\text{Gam}}(v) \approx 0.90e^{-v^{0.96}}v^{1.06} \sim ve^{-v}$ , meaning that the high-speed tail of the distribution  $p(v)$  is approximately exponential. Note here that generalised Gamma speed distributions were also applied to the spreading dynamics of protozoa cells.<sup>29</sup> The distribution  $p(v^2)$  can also be fitted with eqn (17) (not shown). The heavier-than-Gaussian tails were quantified previously, see Fig. 4 in ref. 168. Regarding the nearly exponential tails of the speed distribution we observe for the AX2 strain, Fig. 8 here can be compared with similar  $p(v)$  shapes in Fig. 4F of ref. 65 measured for the AX4 strain of DICTY (we refer also to Fig. 2B and Fig. S1, S4 of ref. 169 and to Fig. 8 of ref. 170 for  $p(v)$  distributions of motile fibroblast cells). The mean instantaneous speed we find for the cells of the AX2 DICTY strain is  $\langle v \rangle \approx 2.3 \mu\text{m min}^{-1}$ .<sup>249</sup>

Finally, the velocity–velocity auto-correlation function<sup>8,100,101,112,113</sup>

$$C_{\text{dt}}(t) = \frac{\langle [\mathbf{r}(t + dt) - \mathbf{r}(t)] \cdot [\mathbf{r}(dt) - \mathbf{r}(0)] \rangle}{(dt)^2} \quad (18)$$

was also computed from the two-dimensional cell traces recorded in our tracking experiments. Here, the time-shift  $dt$  takes a fixed value, the time  $t$  runs along each trace  $\mathbf{r}_i(t)$  until a given time-step, and in (18) averaging is thus performed over initial parts of all the trajectories (to exclude possible effects of ageing and cell slowing-down along the traces). The results of Fig. 15 show that the normalised function,  $C_{\text{dt}}(t)/C_{\text{dt}}(0)$ , decays fast for short times, at  $0 < t < dt$ . Reaching a positive value at time  $t = dt$ , the velocity correlation function starts decaying slower at  $t > dt$ , but remains slightly positive (on average). This feature is consistent with superdiffusive motion: the DICTY cells follow the previous directions of motion statistically more often, but these correlations decay with time (see also Fig. 3 in ref. 46). Experimentally, such persistent behaviour was also observed for the intracellular diffusion of granules in amoeba cells.<sup>7</sup> The typical time of this second decay is  $\sim 5 \dots 10$  steps, or  $\sim 100 \dots 200$  s. The variations of  $C_{\text{dt}}(t)/C_{\text{dt}}(0)$  at longer times are due to insufficient statistics.

Note that the periods of persistent run-and-turn cycles of DICTY were reported to be in the range  $\sim 1 \dots 3$  min.<sup>19,46,47,66</sup> Also, the cell dynamics was shown to reveal more than one internal time scale, with a “knee” in the velocity autocorrelation function at  $\sim 1.5 \dots 2$  min, see Fig. 3 in ref. 51. Note that a persistent walk at short times can differ for longitudinal and transversal directions of cell motion due to a pronounced cell asymmetry.<sup>51,250</sup>

## III. Discussion

Here, we summarise the main results of the current study, discuss their major implications, and scrutinise the mathematical stochastic models that are potentially applicable to describe the observed dynamics of the DICTY cells (the AX2 strain). We quantified the diffusive spreading of the amoeboid cells on two-dimensional surfaces based on (i) the ensemble- and time-averaged MSDs, (ii) the distributions of diffusivities

and scaling exponents of individual cells, (iii) the non-Gaussian distributions of cell displacements, (iv) the long-tail speed distributions of the cells, and (v) the velocity–velocity auto-correlation function. Specifically, we detected (i) and (ii) pronounced heterogeneities and dramatic scatter in the distributions of the diffusion coefficients and scaling exponents along individual trajectories. The ensemble- and time-averaged MSD magnitudes were found not to match each other exactly, manifesting a certain degree of weak non-ergodicity<sup>100,101,103</sup> of an underlying diffusion process. The anomalous scaling exponents decrease from often superdiffusive values at the start to rather small subdiffusive values towards the end of the trajectories. The (iii) DICTY displacements after a given time-shift were found to be severely non-Gaussian, featuring rather close-to-exponential distributions.

Note that additional observables to quantify the features of anomalous diffusion processes are known: (a) the so-called ergodicity breaking parameter,<sup>8,100,101,103</sup> (b) higher-order moments of the distribution of the time-averaged MSD trajectories, such as skewness and kurtosis,<sup>95,174</sup> (c) the non-Gaussianity parameter,<sup>8,105,109</sup> and (d) the shape asymmetry of the trajectory in space.<sup>146</sup> This analysis can be performed in the future, on larger data sets of DICTY positions, recorded for varying experimental conditions and parameters. We refer the reader here also to ref. 107, 108, 112, 135, 146, 149, 151 and 175–181 for a comparative statistical analysis of multiple anomalous-diffusion characteristics, model-comparison tests for single-particle trajectory data (we do not perform such tests here, see ref. 182), and for uncertainties in estimation of the model parameters.

Taken together, the observed features of the DICTY dynamics do not directly match any of the simple standard mathematical models of anomalous diffusion (see also ref. 19). A mixture of two or more stochastic processes of different type is needed, as proposed and considered in ref. 107, 110, 112, 114, 178 and 183–186. Such combined models—for instance, a combination of fractional Brownian motion and continuous time random walks—were already implemented to rationalise experimental data on ageing subdiffusion inside cells,<sup>114</sup> see also ref. 187. To disentangle the sources and origins of underlying stochastic physical processes,<sup>188,189</sup> additional quantitative input from experiments will be required. The key experiments to be done to clarify this have to yield a larger number of longer traces recorded at systematically-varying environment conditions.

The list of conditions includes varying cell densities, ambient temperatures (to probe non-equilibrium features and violations of energy equipartitioning), delay times after the cell culture preparation (possible ageing<sup>46,47</sup> of the DICTY cells), cell adhesion properties onto substrates, *etc.* The implications of surface confinement of the DICTY cells in the lab environment onto the patterns of their three-dimensional motion as occurs *in vivo*—as, *e.g.*, for surface-confined sperm cells<sup>23,190</sup>—may also need quantification. The simultaneous tracking of neighbouring amoebae is highly-desirable to study collective cell-density-dependent behaviours,<sup>6,23,36,145,191</sup> dynamics of moving cell aggregates<sup>192</sup> and mutual cell–cell correlations<sup>193</sup>

(propagating, possibly, *via* hydrodynamic interactions<sup>5,6,16,21,22,35</sup>). This however goes beyond the scope of the present study.

Regarding possible models, the continuous-time random walks<sup>100,101,103,194,195</sup> and heterogeneous diffusion processes<sup>101,136–139</sup> are examples of non-ergodic anomalous diffusion processes with a pronounced spread of time-averaged MSDs. Subdiffusive continuous-time random walks are based on the power-law distribution of waiting times for the next particle jump, namely  $\psi(\tau) \sim 1/\tau^{1+\alpha}$  with  $0 < \alpha < 1$ .<sup>101,103</sup> Heterogeneous diffusion processes describe particle propagation in a medium with position-dependent power-law-varying diffusivity,  $D(x) \sim |x|^{2(\alpha-1)/\alpha}$ . For this choice of the scaling exponent, these two different stochastic processes yield an MSD growth of form (1). For these two processes for the subdiffusive case and in the absence of confinement the MSD scaling exponent is  $0 < \alpha < 1$ , but the time-averaged MSD is always a linear function of the lag time, that is  $\beta = 1$ .<sup>100,101,195</sup> This is not the case for the DICTY diffusion data in Fig. 2a, with the exponents  $\alpha$  and  $\langle\beta\rangle$  being measurably superdiffusive and quite close to one another. Also, the magnitudes of the time-averaged MSD, decreasing with the trajectory length  $T$ , see Fig. 2b and eqn (7), would be characteristic for a subdiffusive process. For superdiffusive stochastic processes one expects rather increasing time-averaged MSD for longer traces, as, for instance, for heterogeneous diffusion processes with  $\alpha > 1$ , where the dependence on the lag time and trace length is  $\langle\overline{\delta_{\text{HDP}}^2(\Delta, T)}\rangle \sim \Delta/T^{1-\alpha}$ , see ref. 136, 137 and 139.

For another class of diffusion processes—namely, for ergodic motion driven by fractional Brownian noise and described by the fractional Langevin equation—the ensemble- and time-averaged MSDs are identical for long trajectories. These processes feature only a tiny spread among independent  $\overline{\delta^2}$  realisations at fixed parameters,<sup>100,101,114,174,176</sup> similar to Brownian motion, both for the amplitudes and scaling exponents. The distribution of particle displacements for these two processes is strictly Gaussian.<sup>101</sup> Our observations in Fig. 2a and 5 indicate, however, a very different behaviour for the DICTY spreading dynamics, thus challenging the applicability of existing anomalous-diffusion models and underlying physical assumptions. In particular, a possible slowing-down or ageing of individual cells after the sample preparation,<sup>47</sup> some intrinsic cell-to-cell variations, population splitting (fast and slow particles<sup>196–198</sup>), environment-induced heterogeneities,<sup>199,200</sup> implications of local and global confinement and compartmentalisation,<sup>138,201</sup> and non-Gaussian displacement distributions (see Appendix B) are the most important new features to be incorporated in future theoretical models for this motile amoeboid system. Given the strong observed heterogeneity of DICTY stochastic properties on the population level, generalised superstatistical or diffusing-diffusivity models may be natural candidates.

Future research should be focused on the understanding of these aspects, to make the current experimental findings and statistical data analysis approaches applicable to other single-cell tracking systems. In general, data sets, where cell densities, growth conditions, culture age, and other environmental factors

are systematically varied, will ultimately provide the answers to these important questions and enable us to pinpoint the best stochastic model underlying the observed DICTY motion.

## IV. Materials and methods

Here, we describe the experimental technique, the data-acquisition strategy, the protocol for measuring cell positions, and the software used for computing and analysing the recorded data. In experiments, we used an AX2 strain of the wild-type DICTY cells cultivated in the HL5 medium (Formedium, Norwich, England) at 22 °C on polystyrene Petri dishes (Primaria, Falcon, BD Becton Dickinson Europe, France), or shaken in suspension at 150 rotations per min. The cells were washed, the HL5 medium was renewed, and then the cells were placed on a plastic Petri dish (Sarstedt, Nümbrecht, Germany) for 30 minutes to allow them to attach to the surface. Polystyrene beads of 15  $\mu\text{m}$  in diameter were placed on the dish as well, as a size reference, see Fig. 1a and the movie in the ESI.† In the analysis of cell positions, only those cells without contacts with the beads were considered. At the start of the single-cell tracking experiment, the cell density was  $\rho \approx 1.2 \times 10^4$  cells per  $\text{cm}^2$  (a rather standard value<sup>19,46,47</sup>), corresponding to the cell-to-cell separation  $\sim 100.70 \mu\text{m}$ .

The DICTY cells are in contact with a polystyrene Petri-dish surface, in contrast to ref. 47 where glass surfaces were used. This can be one of the reasons for the observed differences in the cell diffusivity, in addition to the implications of different cell densities and the DICTY strain used. The environment for cell diffusion is considered to be homogeneous, isotropic, and time-independent (consistent with our data), so that no coordinated DICTY cell-migration patterns or flows occur. Note, however, that even on the homogeneous agar surface the DICTY cells are capable of sensing and following the paths taken by previously diffusing cells, see Fig. 2 in ref. 51.

The recording of cell positions was performed for 6 hours with a bright-field microscope at a frame-rate of  $0.05 \text{ s}^{-1}$ , see Fig. 1a and video files in the ESI.† We track the centre of mass of cells by segmenting the microscopy images first into black-and-white images and then calculating and tracking the centre of mass of every white area. For sedimentation and tracking a custom-made MATLAB algorithm and Image Processing Toolbox were implemented (MathWorks, Ismaning, Germany) using well-established particle-tracking methods.<sup>239,240</sup> The trajectories were analysed afterwards with Mathematica (Wolfram Research Inc., Champaign, USA). In Fig. 1b the cell positions were recorded at different times; crossings of the traces do not imply physical interactions or contacts between the cells, see also ref. 241. We refer the reader to the classical study<sup>46</sup> for the thorough examination of DICTY cell-cell contacts, with broadly-distributed contact durations, lasting on average for 5–10 min (for the NC4 strain).

We monitor the vegetative DICTY cells in the HL5 medium; the cells are  $\sim 15 \mu\text{m}$  in size, but very variable in shape (see video files in the ESI.†). Here, we refer the reader also to Fig. 1A

of ref. 55 illustrating the shape variability for AX2 strain cells. The pixel-width in our microscopy images is  $1 \text{ px} \approx 0.3227 \mu\text{m}$  and the (automatic and manual) accuracy in determining cell positions is  $\sim 0.3 \dots 1 \mu\text{m}$ . The experiments are started 30 minutes after placing the cells on the dish, but the recorded tracks can start at any later time point  $t_{\text{start}}$  during the experiment. Waiting times up to  $t_{\text{start}}$  were not recorded, and thus possible ageing effects on the DICTY dynamics cannot be quantified in our current analysis.

Some cells may be lost during the tracking procedure—some leave the view-field, collide with their neighbours, possibly divide, *etc.*—so the tracking algorithm ceases to distinguish them, see video files in the ESI.† For these events the recorded tracks end, and the cell coordinates start to be recorded again when a new cell emerges in the view-field. Thus, the total number of trajectories we record is about 3 times larger than the number of distinct cells producing the traces. Only trajectories with a minimum number of 60 time-steps were used in the analysis. To improve the statistics of ensemble averaging, longer trajectories in the data set can in principle be segmented into several fragments of the same partial length, see ref. 64, 112 and 242, but we avoid doing so to exclude spurious effects. The reasons are possible ageing, confinement, and non-stationarity effects that can vary along the trajectories, see also Section III.

## Conflicts of interest

There are no conflicts of interest to declare.

## Appendix A: supplementary figures

Here, we collect additional figures to support the claims in the main text of the paper. The length distribution of the recorded DICTY traces is shown in Fig. 9. The distributions of the computed short-time scaling exponents and generalised diffusion coefficients are presented in Fig. 10 and 11, respectively. The evolution of the non-Gaussian displacement distributions of DICTY cells along the  $y$ -direction for varying time-shifts  $\delta t$  is

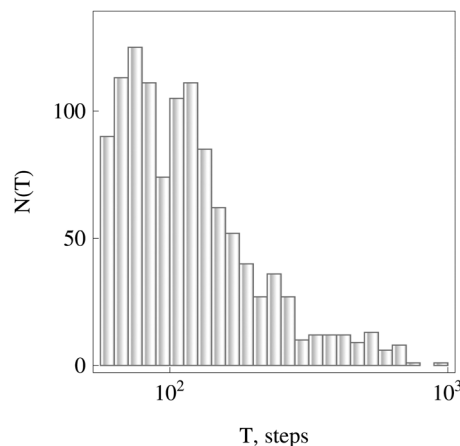


Fig. 9 Length distribution of recorded DICTY trajectories, shown as counts on a linear–log scale (one step is  $\delta t = 20 \text{ s}$ ).

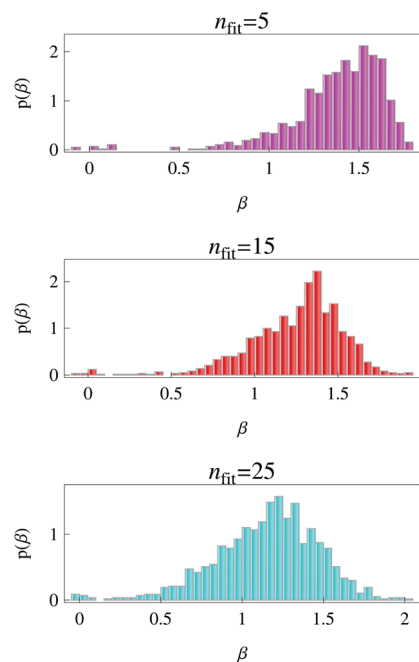


Fig. 10 Probability distribution  $p(\beta)$  of the scaling exponents of time-averaged MSDs for the data set of Fig. 2, computed for  $n_{\text{fit}} = \{5, 15, 25\}$  initial points of  $\overline{\delta^2(A)}$  trajectories.

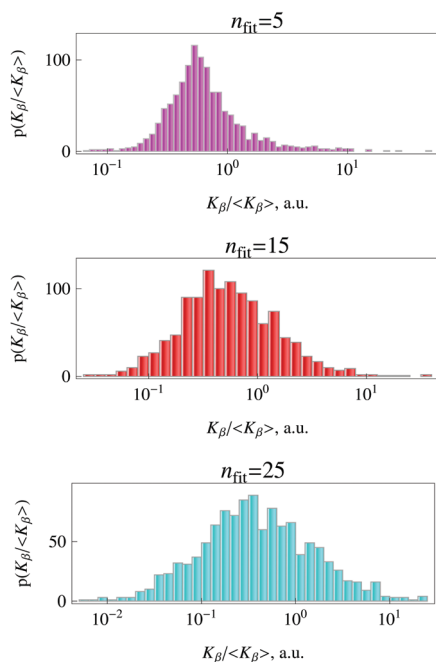


Fig. 11 Distribution of generalised diffusion coefficients,  $K_{\beta}/\langle K_{\beta} \rangle$ , for the data set of Fig. 2, in the same colour scheme as in Fig. 10.

illustrated in Fig. 12. The distributions of cell displacements along the  $x$ -direction are shown in Fig. 13 on a linear scale. The power-law scaling of the width of displacement distributions with varying time-shifts,  $\sigma(\delta t)$ , is presented in Fig. 6. The velocity–velocity correlation function for varying time-shifts (in steps) is shown in Fig. 15.

## Appendix B: non-Gaussianity and diffusing diffusivity

Here, we provide an overview of non-Gaussian behaviours observed recently for other biological and cell-related systems featuring normal and anomalous diffusion. The issue of non-Gaussian displacement distributions  $p(\delta x)$  originated from the by-now seminal works of Granick *et al.*<sup>160,161,202</sup> Namely, they observed that fluorescently-tagged unilamellar lipid vesicles diffusing in nematic solutions of F-actin filaments exhibit Fickian yet non-Gaussian diffusion.<sup>161</sup> The linear MSD growth was shown to coexist with exponential rather than Gaussian  $p(\delta x)$ . Since then, the concepts of distributed/fluctuating diffusivity and non-Gaussian  $p(\delta x)$  have led to flourishing progress of experimental,<sup>8,16,29,95,108,112,159,201,203–221</sup> theoretical,<sup>163–166,222–228</sup> and computer simulation<sup>109,111,229–234</sup> studies (see also the earlier study of non-Gaussian effects in complex heterogeneous media and gels<sup>145</sup>). Varying diffusivities were detected, *i.a.*, for lateral subdiffusion of lipids, proteins, and water molecules along<sup>231,234–236</sup> and for permeation of small molecules across<sup>232</sup> lipid membranes.

We touch here on a few recent biological examples of non-Gaussianity. (i) Ergodic and non-ergodic motions of Kv2.1 channels on plasma membranes of human embryonic kidney cells were found by Krapf *et al.* to coexist.<sup>237</sup> The distribution function of particle displacements was non-Gaussian, with a pronounced peak at small displacements and a broad spread of diffusivities,  $p(K_{\beta})$ .<sup>237</sup> (ii) For intracellular subdiffusive non-ergodic ageing motion of insulin granules in pancreatic  $\beta$ -cells the distributions  $p(\delta x)$  were shown to have non-Gaussian long-tail statistics, with strongly enhanced probabilities of large displacements. Similar to our observations for DICTY cells in Fig. 2a, the individual time-averaged MSD traces were shown to feature a wide spread of  $K_{\beta}$  (consistent with a continuous-time random walk mechanism and indicating system heterogeneities). However, rather “stable” scaling exponents along each time-averaged MSD trace were detected, with  $\beta(A) \sim 0.7 \dots 0.8$ ,<sup>114</sup> indicative rather of fractional Brownian motion. The ageing behaviour in ref. 114 was consistent with a decaying magnitude of time-averaged MSDs with trace length  $T$  of the form  $\langle \overline{\delta^2(A)} \rangle \sim 1/T^{1-\beta}$ ,<sup>114</sup> characteristic again for (ageing) subdiffusive continuous-time random walks.<sup>197,198</sup> A “hybrid” model incorporating the features of these two processes was proposed to rationalise the observed granule dynamics.<sup>114</sup> (iii) Superdiffusive motion of the membrane-targeting C2 domains on supported lipid bilayers<sup>212</sup> was shown to emerge due to bulk-mediated particle excursions. The non-Gaussian distribution  $p(\delta x)$  was fitted with a combination of a two-dimensional Gaussian propagator for surface-mediated diffusion and a Cauchy function describing long-distance hops.<sup>212</sup> (iv) For aqueous solutions crowded with entangled dextran molecules, the MSD of diffusing proteins was measured to grow linearly and ergodically with time, whereas the propagator of particle displacements at short length-scales was non-Gaussian.<sup>210</sup> (v) The dynamics of nanoparticles in microfabricated arrays of nanoposts was shown

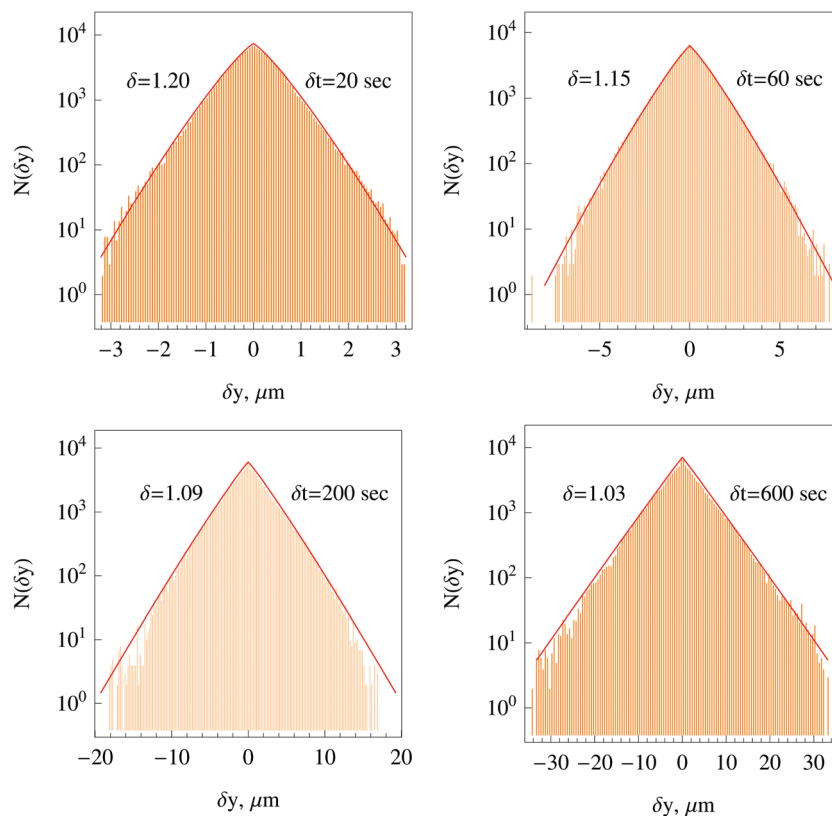


Fig. 12 The same as in Fig. 5, but for cell displacements along the y direction.

to yield a Brownian MSD growth, but a stretched-Gaussian  $p(\delta x)$  distribution.<sup>211</sup> (vi) The spreading of polyethylene-glycol polymers on nanopatterned surfaces was found to be slightly subdiffusive,<sup>205</sup> but featuring strongly non-Gaussian step-size distributions. A sharp peak at small displacements was attributed to a subpopulation of immobile chains and long tails of  $p(\delta x)$  distributions were shown to feature a non-Fickian scaling for their width.<sup>205</sup> (vii) The diffusion of polymers and some proteins along a solid–liquid interface was shown by Schwartz *et al.*<sup>216,218,220</sup> to have a pronounced spike in the van Hove correlation function  $G_s(\delta x)$  for small displacements (due to confined motion). Slower-than-Gaussian tails of  $G_s(\delta x)$  were shown to coexist with a weakly subdiffusive or normal MSD growth of the particles.<sup>216,218</sup> (viii) A slower-than-Gaussian decay and linear MSD growth were also detected for nanoparticle diffusion in porous 3D media,<sup>219</sup> with likely heterogeneous and space-dependent mobilities of the particles.

(ix) We describe now one recent example of a non-Gaussian distribution  $G_s(\delta x)$  in detail. The rescaling of the width of DICTY displacement distributions we observe is similar to the non-Gaussian fat-tail behaviour detected by Spakowitz *et al.*<sup>159</sup> They quantified subdiffusive non-ergodic motion of RNA–protein complexes (tracers) in the cytoplasm of *Escherichia coli* and *Saccharomyces cerevisiae* cells. Heterogeneous features of the cytoplasm and variations of diffusion characteristics were probed, see also ref. 165. The authors demonstrated a close-to-exponential  $\pi(K_z)$  distribution of tracer diffusivities and the existence

of a scaling variable  $z = \delta x / (\delta t)^{\alpha/2}$ , similar to our eqn (13). Then, convoluting the exponential distribution,<sup>163,164</sup>  $\pi(K_z) = 1/\langle K_z \rangle \exp[-K_z/\langle K_z \rangle]$ , with the Gaussian propagator for a given diffusivity,

$$P(\delta x, \delta t, K_z) = \frac{1}{\sqrt{4\pi K_z (\delta t)^z}} \exp\left[-\frac{(\delta x)^2}{4K_z (\delta t)^z}\right], \quad (\text{B1})$$

one can arrive at an exponential distribution,<sup>159</sup>

$$P(\delta x, \delta t) = \int_0^\infty \pi(K_z) P(\delta x, \delta t, K_z) dK_z \\ = \frac{1}{\sqrt{4\langle K_z \rangle (\delta t)^z}} \exp\left[-\frac{|\delta x|^1}{\sqrt{\langle K_z \rangle (\delta t)^z}}\right]. \quad (\text{B2})$$

The observations of ref. 159 agree with the theoretical predictions.<sup>161,163–165</sup> Note that for subdiffusive motion of chromosomal loci the same group detected a wide spread of diffusivities  $K_\beta$  and scaling exponents  $\beta$ .<sup>115</sup> The reader is referred to ref. 164 and 238 for more examples of non-Gaussianity. (x) The diffusion of nematode *Phasmarhabditis hermaphrodita* in heterogeneous populations on agar plates was shown to be normal at the level of individual worms, but overall anomalous spreading with broadly-distributed diffusivities was detected.<sup>162</sup> The Gamma-distribution  $\pi_{\text{Gam}}(D)$  was used to fit it. The distribution of displacements in an ensemble of worms was shown to have a pronounced longer-than-Gaussian (exponential) tail.<sup>162</sup>

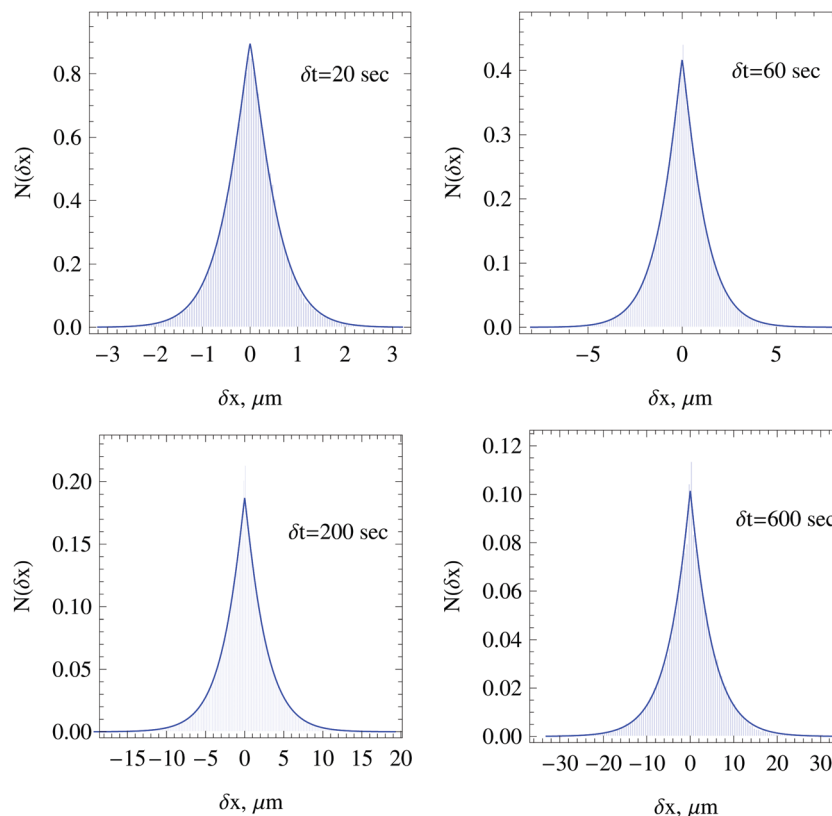


Fig. 13 The data set for cell displacements of Fig. 5, but presented as the probability distribution on a linear scale.

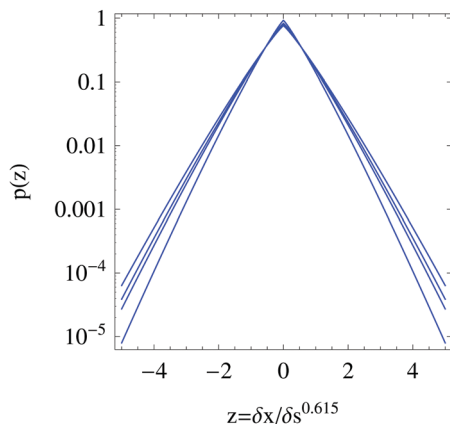


Fig. 14 The same as in Fig. 7 but on a semi-log scale.

Some computational and theoretical examples of non-Gaussian  $p(\delta x)$  are as follows. (i) Recent computer simulations of anomalous non-ergodic subdiffusion of phospholipids and proteins in viscoelastic environments of crowded lipid membranes by Vattulainen *et al.* revealed a number of pronounced non-Gaussian features.<sup>111</sup> (ii) The dynamics of membrane-binding proteins interacting with specific lipids was shown—*via* coarse-grained Molecular Dynamics simulations—to induce a fluctuating-diffusivity landscape.<sup>234</sup> The diffusion of protein domains remained ergodic, but featuring temporally-fluctuating short-time diffusivities. Moreover, a longer-than-Gaussian tail in  $p(\delta x)$  was detected in this *in silico* study.<sup>234</sup>

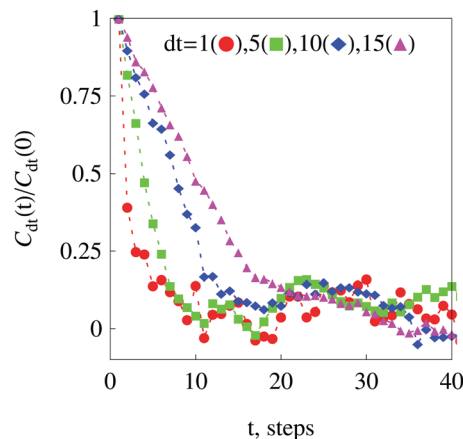


Fig. 15 Velocity auto-correlation function (18) plotted for different time-shifts  $dt$  (one step is 20 s).

(iii) Recent simulations of tracer diffusion in heterogeneously-crowded circular domains—mimicking macromolecular crowding inside eukaryotic cells—was shown to reveal non-Gaussian and anomalous-diffusion features.<sup>109</sup> (iv) We refer the reader to the superstatistics-based study<sup>164</sup> where the mathematical framework was developed for the analysis of MSDs and displacement distributions in the systems with fluctuating diffusivities. (v) Lastly, anomalous and non-Gaussian diffusion in non-stationary time-fluctuating diffusivity landscapes with the Rayleigh-like distribution of diffusivities  $\pi_{\text{Ray}}(D)$  was examined in ref. 227 by computer simulations.

## Acknowledgements

We thank H. Flyvbjerg for useful comments on the final version of the manuscript. RM and CB acknowledge financial support from the Deutsche Forschungsgemeinschaft, DFG Projects ME 1535/6-1, ME 1535/7-1, and BE 3978/10-1. RM also acknowledges support within Alexander von Humboldt Polish Honorary Research Scholarship. This research was partially funded by the Grant CRC 1294 “Data Assimilation-The seamless integration of data and models” (SFB 1294 of Deutsche Forschungsgemeinschaft, to CB) and Project B02 “Inferring the dynamics underlying protrusion-driven cell motility” (to CB).

## References

- 1 C. Bechinger, R. Di Leonardo, H. Löwen, C. Reichhardt, G. Volpe and G. Volpe, Active particles in complex and crowded environments, *Rev. Mod. Phys.*, 2016, **88**, 045006.
- 2 *Physical models of cell motility*, ed. I. S. Aronson, Springer, 2016.
- 3 J. Prost, F. Jülicher and J.-F. Joanny, Active gel physics, *Nat. Phys.*, 2015, **11**, 111.
- 4 A. M. Menzel, Tuned, driven, and active soft matter, *Phys. Rep.*, 2015, **554**, 1.
- 5 X.-L. Wu and A. Libchaber, Particle diffusion in a quasi-two-dimensional bacterial bath, *Phys. Rev. Lett.*, 2000, **84**, 3017.
- 6 A. Zöttl and H. Stark, Emergent behavior in active colloids, *J. Phys.: Condens. Matter*, 2016, **28**, 253001.
- 7 J. F. Reverey, J.-H. Jeon, H. Bao, M. Leippe, R. Metzler and C. Selhuber-Unkel, Superdiffusion dominates intracellular particle motion in the supercrowded cytoplasm of pathogenic *Acanthamoeba castellanii*, *Sci. Rep.*, 2015, **5**, 11690.
- 8 K. Norregaard, R. Metzler, C. M. Ritter, K. Berg-Sørensen and L. B. Oddershede, Manipulation and motion of organelles and single molecules in living cells, *Chem. Rev.*, 2017, **117**, 4342.
- 9 V. Hakim and P. Silberzan, Collective cell migration: a physics perspective, *Rep. Progr. Phys.*, 2017, **80**, 076601.
- 10 F. Ziebert and I. S. Aronson, Computational approaches to substrate-based cell motility, *npj Comput. Mater.*, 2016, **2**, 16019.
- 11 T. J. Mitchison and L. P. Cramer, Actin-based cell motility and cell locomotion, *Cell*, 1996, **84**, 371.
- 12 P. Maiuri, *et al.*, The first world cell race, *Curr. Biol.*, 2012, **22**, R673.
- 13 P. Maiuri, J.-F. Rupprecht, S. Wieser, V. Rupprecht, O. Benichou, N. Carpi, M. Coppey, S. De Beco, N. Gov, C.-Ph. Heisenberg, C. L. Crespo, F. Lautenschlaeger, M. Le Berre, A.-M. Lennon-Dumenil, M. Raab, H.-R. Thiam, M. Piel, M. Sixt and R. Voituriez, Actin flows mediate a universal coupling between cell speed and cell persistence, *Cell*, 2015, **161**, 374.
- 14 O. Chepizhko, C. Giampietro, E. Mastrapasqua, M. Nourazar, M. Ascagni, M. Sugni, U. Fascio, L. Leggio, C. Malinverno, G. Scita, S. Santucci, M. J. Alava, S. Zapperi and C. A. M. La Porta, Bursts of activity in collective cell migration, *Proc. Natl. Acad. Sci. U. S. A.*, 2016, **113**, 11408.
- 15 H. C. Berg and D. A. Brown, Chemotaxis in *Escherichia coli* analysed by three-dimensional tracking, *Nature*, 1972, **239**, 500.
- 16 G. Ariel, A. Rabani, S. Benisty, J. D. Partridge, R. M. Harshey and A. Be'er, Swarming bacteria migrate by Lévy walk, *Nat. Commun.*, 2015, **6**, 8396.
- 17 R. Marathe, C. Meel, N. C. Schmidt, L. Dewenter, R. Kurre, L. Greune, M. A. Schmidt, M. J. I. Müller, R. Lipowsky, B. Maier and S. Klumpp, Bacterial twitching motility is coordinated by a two-dimensional tug-of-war with directional memory, *Nat. Commun.*, 2014, **5**, 3759.
- 18 H. Koorehdavoudi, P. Bogdan, G. Wei, R. Marculescu, J. Zhuang, R. W. Carlsen and M. Sitti, Multi-fractal characterization of bacterial swimming dynamics: a case study on real and simulated *Serratia marcescens*, *Proc. R. Soc. A*, 2017, **473**, 20170154.
- 19 L. Li, S. F. Nørrelykke and E. C. Cox, Persistent cell motion in the absence of external signals: a search strategy for eukaryotic cells, *PLoS One*, 2008, **3**, e2093.
- 20 P. Romanczuk, M. Bär, W. Ebeling, B. Lindner and L. Schimansky-Geier, Active Brownian particles, *Eur. Phys. J.: Spec. Top.*, 2012, **202**, 1.
- 21 M. C. Marchetti, J.-F. Joanny, S. Ramaswamy, T. B. Liverpool, J. Prost, M. Rao and R. A. Simha, Hydrodynamics of soft active matter, *Rev. Mod. Phys.*, 2013, **85**, 1143.
- 22 E. Lauga and T. R. Powers, The hydrodynamics of swimming microorganisms, *Rep. Prog. Phys.*, 2009, **72**, 096601.
- 23 J. Elgeti, R. G. Winkler and G. Gompper, Physics of microswimmers—single particle motion and collective behavior: a review, *Rep. Prog. Phys.*, 2015, **78**, 056601.
- 24 R. G. Winkler, J. Elgeti and G. Gompper, Active polymers—emergent conformational and dynamical properties: a brief review, *J. Phys. Soc. Jpn.*, 2017, **86**, 101014.
- 25 N. Koumakis, A. Lepore, C. Maggi and R. Di Leonardo, Targeted delivery of colloids by swimming bacteria, *Nat. Commun.*, 2013, **4**, 2588.
- 26 A. Upadhyaya, J.-P. Rieu, J. A. Glazier and Y. Sawada, Anomalous diffusion and non-Gaussian velocity distribution of *Hydra* cells in cellular aggregates, *Phys. A*, 2001, **293**, 549.
- 27 M. Theves, J. Taktikos, V. Zaburdaev, H. Stark and C. Beta, A bacterial swimmer with two alternating speeds of propagation, *Biophys. J.*, 2013, **105**, 1915.
- 28 D. Cuvelier, M. Thery, Y.-S. Chu, S. Dufour, J.-P. Thiery, M. Bornens, P. Nassoy and L. Mahadevan, The universal dynamics of cell spreading, *Curr. Biol.*, 2007, **17**, 694.
- 29 L. G. A. Alves, D. B. Scariot, R. R. Guimaraes, C. V. Nakamura, R. S. Mendes and H. V. Ribeiro, Transient superdiffusion and long-range correlations in the motility patterns of trypanosomatid flagellate protozoa, *PLoS One*, 2016, **11**, e0152092.
- 30 J. de Anda, E. Y. Lee, C. K. Lee, R. R. Bennett, X. Ji, S. Soltani, M. C. Harrison, A. E. Baker, Y. Luo, T. Chou, G. A. O'Toole, A. M. Armani, R. Golestanian and

- G. C. L. Wong, High-speed “4D” computational microscopy of bacterial surface motility, *ACS Nano*, 2017, **11**, 9340.
- 31 A. C. H. Tsang, A. T. Lam and I. H. Riedel-Kruse, Polygonal motion and adaptable phototaxis via flagellar beat switching in *Euglena gracilis*, bioRxiv, DOI: 10.1101/292896.
- 32 A. E. Patteson, A. Gopinath, P. K. Purohit and P. E. Arratia, Particle diffusion in active fluids is non-monotonic in size, *Soft Matter*, 2016, **12**, 2365.
- 33 E. Ben-Jacob, I. Cohen and H. Levine, Cooperative self-organization of microorganisms, *Adv. Phys.*, 2000, **49**, 395.
- 34 A. Sokolov, I. S. Aranson, J. O. Kessler and R. E. Goldstein, Concentration dependence of the collective dynamics of swimming bacteria, *Phys. Rev. Lett.*, 2007, **98**, 158102.
- 35 T. Ala-Nissila, R. Ferrando and S. C. Ying, Collective and single particle diffusion on surfaces, *Adv. Phys.*, 2002, **51**, 949.
- 36 T. Vicsek and A. Zafeiris, Collective motion, *Phys. Rep.*, 2012, **517**, 71.
- 37 P. J. Albert and U. S. Schwarz, Dynamics of cell ensembles on adhesive micropatterns: bridging the gap between single cell spreading and collective cell migration, *PLoS Comput. Biol.*, 2016, **12**, e1004863.
- 38 A. Huttenlocher, R. R. Sandborg and A. F. Horwitz, Adhesion in cell migration, *Curr. Opin. Cell Biol.*, 1995, **7**, 697.
- 39 D. A. Lauffenburger and A. F. Horwitz, Cell migration: a physically integrated molecular process, *Cell*, 1996, **84**, 359.
- 40 P. Friedl and K. Wolf, Tumour-cell invasion and migration: diversity and escape mechanisms, *Nat. Rev. Cancer*, 2003, **3**, 362.
- 41 K. Wolf, I. Mazo, H. Leung, K. Engelke, U. H. von Andrian, E. I. Deryugina, A. Y. Strongin, E.-B. Bröcker and P. Friedl, Compensation mechanism in tumor cell migration: mesenchymal-amoeboid transition after blocking of pericellular proteolysis, *J. Cell Biol.*, 2003, **160**, 267.
- 42 D. Hanahan and R. A. Weinberg, The hallmarks of cancer: the next generation, *Cell*, 2011, **144**, 646.
- 43 A. Fritsch, M. Höckel, T. Kiessling, K. D. Nnetu, F. Wetzel, M. Zink and J. A. Käs, Are biomechanical changes necessary for tumour progression?, *Nat. Phys.*, 2010, **6**, 730.
- 44 A. W. Holle, M. Kalafat, A. S. Ramos, T. Seufferlein, R. Kemkemer and J. P. Spatz, Intermediate filament reorganization dynamically influences cancer cell alignment and migration, *Sci. Rep.*, 2017, **7**, 45152.
- 45 A.-K. V. West, L. Wullkopf, A. Christensen, N. Leijnse, J. M. Tarp, J. Mathiesen, J. T. Erler and L. B. Oddershede, Dynamics of cancerous tissue correlates with invasiveness, *Sci. Rep.*, 2017, **7**, 43800.
- 46 M. J. Potel and S. A. Mackay, Preaggregative cell motion in *Dictyostelium*, *J. Cell Sci.*, 1979, **36**, 281.
- 47 L. Gole, C. Riviere, Y. Hayakawa and J.-P. Rieu, A quorum-sensing factor in vegetative *Dictyostelium discoideum* cells revealed by quantitative migration analysis, *PLoS One*, 2011, **6**, e26901.
- 48 T. Gregor, K. Fujimoto, N. Masaki and S. Sawai, The onset of collective behavior in social amoebae, *Science*, 2010, **328**, 1021.
- 49 C. Westendorf, J. Negrete, Jr., A. J. Bae, R. Sandmann, E. Bodenschatz and C. Beta, Actin cytoskeleton of chemotactic amoebae operates close to the onset of oscillations, *Proc. Natl. Acad. Sci. U. S. A.*, 2013, **110**, 3853.
- 50 G. Gerisch, Chemotaxis in *Dictyostelium*, *Annu. Rev. Physiol.*, 1982, **44**, 535.
- 51 L. Li, E. C. Cox and H. Flyvbjerg, “Dicty dynamics”: *Dictyostelium* motility as persistent random motion, *Phys. Biol.*, 2011, **8**, 046006.
- 52 J. M. E. Nichols, D. Veltman and R. R. Kay, Chemotaxis of a model organism: progress with *Dictyostelium*, *Curr. Opin. Cell Biol.*, 2015, **36**, 7.
- 53 G. Amselem, M. Theves, A. Bae, E. Bodenschatz and C. Beta, A stochastic description of *Dictyostelium* chemotaxis, *PLoS One*, 2012, **7**, e37213.
- 54 L. L. Song, S. M. Nadkarni, H. U. Bodeker, C. Beta, A. Bae, C. Franck, W. J. Rappel, W. F. Loomis and E. Bodenschatz, *Dictyostelium discoideum* chemotaxis: threshold for directed motion, *Eur. J. Cell Biol.*, 2006, **85**, 981.
- 55 L. Tweedy, B. Meier, J. Stephan, D. Heinrich and R. G. Endres, Distinct cell shapes determine accurate chemotaxis, *Sci. Rep.*, 2013, **3**, 2606.
- 56 G. Aquino, L. Tweedy, D. Heinrich and R. G. Endres, Memory improves precision of cell sensing in fluctuating environments, *Sci. Rep.*, 2014, **4**, 5688.
- 57 Y. Cheng and H. Othmer, A model for direction sensing in *Dictyostelium discoideum*: Ras activity and symmetry breaking driven by a  $G_{\beta\gamma}$ -mediated,  $G_{\alpha 2}$ -Ric8—dependent signal transduction network, *PLoS Comput. Biol.*, 2016, **12**, e1004900.
- 58 D. A. Brock, T. E. Douglas, D. C. Queller and J. E. Strassmann, Primitive agriculture in a social amoeba, *Nature*, 2011, **469**, 393.
- 59 J. Käfer, P. Hogeweg and A. F. M. Maree, Moving forward moving backward: directional sorting of chemotactic cells due to size and adhesion differences, *PLoS Comput. Biol.*, 2006, **2**, e56.
- 60 C. Beta, G. Amselem and E. Bodenschatz, A bistable mechanism for directional sensing, *New J. Phys.*, 2008, **10**, 083015.
- 61 C. Beta and E. Bodenschatz, Microfluidic tools for quantitative studies of eukaryotic chemotaxis, *Eur. J. Cell Biol.*, 2011, **90**, 811.
- 62 G. Amselem, M. Theves, A. Bae, C. Beta and E. Bodenschatz, Control parameter description of eukaryotic chemotaxis, *Phys. Rev. Lett.*, 2012, **109**, 108103.
- 63 C. Guven, E. Rericha, E. Ott and W. Losert, Modeling and measuring signal relay in noisy directed migration of cell groups, *PLoS Comput. Biol.*, 2013, **9**, e1003041.
- 64 Z. Eidi, F. Mohammad-Rafiee, M. Khorrami and A. Gholami, Modelling of *Dictyostelium discoideum* movement in linear gradient of chemoattractant, *Soft Matter*, 2017, **13**, 8209.
- 65 D. Selmeczi, L. Li, L. I. I. Pedersen, S. F. Norrelykke, P. H. Hagedorn, S. Mosler, N. B. Larsen, E. C. Cox and

- H. Flyvbjerg, Cell motility as random motion: a review, *Eur. Phys. J.: Spec. Top.*, 2008, **157**, 1.
- 66 A. D. Shenderov and M. P. Sheetz, Inversely correlated cycles in speed and turning in an ameba: an oscillatory model of cell locomotion, *Biophys. J.*, 1997, **72**, 2382.
- 67 M. Levandowsky, B. White and F. L. Schuster, Random movements of soil amoebas, *Acta Protozool.*, 1997, **36**, 237.
- 68 A. Bhowmik, W.-J. Rappel and H. Levine, Excitable waves and direction-sensing in *Dictyostelium discoideum*: steps towards a chemotaxis model, *Phys. Biol.*, 2016, **13**, 016002.
- 69 V. Lakhani and T. C. Elston, Testing the limits of gradient sensing, *PLoS Comput. Biol.*, 2017, **13**, e1005386.
- 70 I. Niculescu, J. Textor and R. J. de Boer, Crawling and gliding: a computational model for shape-driven cell migration, *PLoS Comput. Biol.*, 2015, **11**, e1004280.
- 71 P. J. M. van Haastert, A model for a correlated random walk based on the ordered extension of pseudopodia, *PLoS Comput. Biol.*, 2010, **6**, e1000874.
- 72 J. S. King and R. H. Insall, Chemotaxis: finding the way forward with *Dictyostelium*, *Trends Cell Biol.*, 2009, **19**, 523.
- 73 H. Ebata, A. Yamamoto, Y. Tsuji, S. Sasaki, K. Moriyama, T. Kuboki and S. Kidoaki, Persistent random deformation model of cells crawling on a gel surface, *Sci. Rep.*, 2018, **8**, 5153.
- 74 O. Nagel, C. Guven, M. Theves, M. Driscoll, W. Losert and C. Beta, Geometry-driven polarity in motile amoeboid cells, *PLoS One*, 2014, **9**, e113382.
- 75 N. Makarava, S. Menz, M. Theves, W. Huisinga, C. Beta and M. Holschneider, Quantifying the degree of persistence in random amoeboid motion based on the Hurst exponent of fractional Brownian motion, *Phys. Rev. E*, 2014, **90**, 042703.
- 76 A. Mogilner, Mathematics of cell motility: have we got its number?, *J. Math. Biol.*, 2009, **58**, 105.
- 77 C. Beta and K. Kruse, Intracellular oscillations and waves, *Annu. Rev. Condens. Matter Phys.*, 2017, **8**, 239.
- 78 Y. Artemenko, T. J. Lampert and P. N. Devreotes, Moving towards a paradigm: common mechanisms of chemotactic signaling in *Dictyostelium* and mammalian leukocytes, *Cell. Mol. Life Sci.*, 2014, **71**, 3711.
- 79 M. K. Driscoll, C. McCann, R. Kopace, T. Homan, J. T. Fourkas, C. Parent and W. Losert, Cell shape dynamics: from waves to migration, *PLoS Comput. Biol.*, 2012, **8**, e1002392.
- 80 H. Leonhardt, M. Gerhardt, N. Höppner, K. Krüger, M. Tarantola and C. Beta, Cell-substrate impedance fluctuations of single amoeboid cells encode cell-shape and adhesion dynamics, *Phys. Rev. E*, 2016, **93**, 012414.
- 81 S. Huth, J. F. Reverey, M. Leippe and C. Selhuber-Unkel, Adhesion forces and mechanics in mannose-mediated *acanthamoeba* interactions, *PLoS One*, 2017, **12**, e0176207.
- 82 P. J. M. van Haastert and L. Bosgraaf, Food searching strategy of amoeboid cells by starvation induced run length extension, *PLoS One*, 2009, **4**, e6814.
- 83 V. V. Palyulin, A. V. Chechkin and R. Metzler, Lévy flights do not always optimize random blind search for sparse targets, *Proc. Natl. Acad. Sci. U. S. A.*, 2014, **111**, 2931.
- 84 G. Volpe and G. Volpe, The topography of the environment alters the optimal search strategy for active particles, *Proc. Natl. Acad. Sci. U. S. A.*, 2017, **114**, 11350.
- 85 L. G. A. Alves, P. B. Winter, L. N. Ferreira, R. M. Brielmann, R. I. Morimoto and L. A. N. Amaral, Long-range correlations and fractal dynamics in *C. elegans*: changes with aging and stress, *Phys. Rev. E*, 2017, **96**, 022417.
- 86 H. Miyoshi, N. Masaki and Y. Tsuchiya, Characteristics of trajectory in the migration of *Amoeba proteus*, *Protoplasma*, 2003, **222**, 175.
- 87 C. P. Brangwynne, G. H. Koenderink, F. C. MacKintosh and D. A. Weitz, Intracellular transport by active diffusion, *Trends Cell Biol.*, 2009, **19**, 423.
- 88 M. Guo, A. J. Ehrlicher, M. H. Jensen, M. Renz, J. R. Moore, R. D. Goldman, J. Lippincott-Schwartz, F. C. Mackintosh and D. A. Weitz, Probing the stochastic, motor-driven properties of the cytoplasm using force spectrum microscopy, *Cell*, 2014, **158**, 822.
- 89 D. Arcizet, B. Meier, E. Sackmann, J. O. Rädler and D. Heinrich, Temporal analysis of active and passive transport in living cells, *Phys. Rev. Lett.*, 2008, **101**, 248103.
- 90 C. Wilhelm, Out-of-equilibrium microrheology inside living cells, *Phys. Rev. Lett.*, 2008, **101**, 028101.
- 91 E. Fodor, C. Nardini, M. E. Cates, J. Tailleur, P. Visco and F. van Wijland, How far from equilibrium is active matter?, *Phys. Rev. Lett.*, 2016, **117**, 038103.
- 92 F. Gnesotto, F. Mura, J. Gladrow and C. P. Broedersz, Broken detailed balance and non-equilibrium dynamics in living systems, *Rep. Prog. Phys.*, 2018, **81**, 066601.
- 93 A. Caspi, R. Granek and M. Elbaum, Enhanced diffusion in active intracellular transport, *Phys. Rev. Lett.*, 2000, **85**, 5655.
- 94 A. Caspi, R. Granek and M. Elbaum, Diffusion and directed motion in cellular transport, *Phys. Rev. E*, 2002, **66**, 011916.
- 95 P. Dieterich, R. Klages, R. Preuss and A. Schwab, Anomalous dynamics of cell migration, *Proc. Natl. Acad. Sci. U. S. A.*, 2008, **105**, 459.
- 96 M. S. Song, H. C. Moon, J.-H. Jeon and H. Y. Park, Neuronal messenger ribonucleoprotein transport follows an aging Lévy walk, *Nat. Commun.*, 2018, **9**, 344.
- 97 I. M. Zaid, J. Dunkel and J. M. Yeomans, Lévy fluctuations and mixing in dilute suspensions of algae and bacteria, *J. R. Soc., Interface*, 2011, **8**, 1314.
- 98 J.-P. Bouchaud and A. Georges, Anomalous diffusion in disordered media: Statistical mechanisms, models and physical applications, *Phys. Rep.*, 1990, **195**, 127.
- 99 M. J. Saxton and K. Jacobson, Single-particle tracking: applications to membrane dynamics, *Annu. Rev. Biophys. Biomol. Struct.*, 1997, **26**, 373.
- 100 S. Burov, J.-H. Jeon, R. Metzler and E. Barkai, Single particle tracking in systems showing anomalous diffusion: the role of weak ergodicity breaking, *Phys. Chem. Chem. Phys.*, 2011, **13**, 1800.

- 101 R. Metzler, J.-H. Jeon, A. G. Cherstvy and E. Barkai, Anomalous diffusion models and their properties: non-stationarity, non-ergodicity, and ageing at the centenary of single particle tracking, *Phys. Chem. Chem. Phys.*, 2014, **16**, 24128.
- 102 E. Barkai, Y. Garini and R. Metzler, Strange kinetics of single molecules in living cells, *Phys. Today*, 2012, **65**(8), 29.
- 103 Y. He, S. Burov, R. Metzler and E. Barkai, Random timescale invariant diffusion and transport coefficients, *Phys. Rev. Lett.*, 2008, **101**, 058101.
- 104 I. M. Sokolov, Models of anomalous diffusion in crowded environments, *Soft Matter*, 2012, **8**, 9043.
- 105 F. Höfling and T. Franosch, Anomalous transport in the crowded world of biological cells, *Rep. Prog. Phys.*, 2013, **76**, 046602.
- 106 A. Bodrova, A. V. Chechkin, A. G. Cherstvy, H. Safdari, I. M. Sokolov and R. Metzler, Underdamped scaled Brownian motion: (non-)existence of the overdamped limit in anomalous diffusion, *Sci. Rep.*, 2016, **6**, 30520.
- 107 Y. Meroz and I. M. Sokolov, A toolbox for determining subdiffusive mechanisms, *Phys. Rep.*, 2015, **573**, 1.
- 108 N. Gal, D. Lechtman-Goldstein and D. Weihs, Particle tracking in living cells: a review of the mean square displacement method and beyond, *Rheol. Acta*, 2013, **52**, 425.
- 109 S. K. Ghosh, A. G. Cherstvy, D. S. Grebenkov and R. Metzler, Anomalous, non-Gaussian tracer diffusion in crowded two-dimensional environments, *New J. Phys.*, 2016, **18**, 013027.
- 110 P. C. Bressloff and J. M. Newby, Stochastic models of intracellular transport, *Rev. Mod. Phys.*, 2013, **85**, 135.
- 111 J.-H. Jeon, M. Javanainen, H. Martinez-Seara, R. Metzler and I. Vattulainen, Protein crowding in lipid bilayers gives rise to non-Gaussian anomalous lateral diffusion of phospholipids and proteins, *Phys. Rev. X*, 2016, **6**, 021006.
- 112 Y. Golan and E. Sherman, Resolving mixed mechanisms of protein subdiffusion at the T cell plasma membrane, *Nat. Commun.*, 2017, **8**, 15851.
- 113 J.-H. Jeon, V. Tejedor, S. Burov, E. Barkai, C. Selhuber-Unkel, K. Berg-Sorensen, L. Oddershede and R. Metzler, *In vivo* anomalous diffusion and weak ergodicity breaking of lipid granules, *Phys. Rev. Lett.*, 2011, **106**, 048103.
- 114 S. M. A. Tabei, S. Burov, H. Y. Kim, A. Kuznetsov, T. Huynh, J. Jureller, L. H. Philipson, A. R. Dinner and N. F. Scherer, Intracellular transport of insulin granules is a subordinated random walk, *Proc. Natl. Acad. Sci. U. S. A.*, 2013, **110**, 4911.
- 115 S. C. Weber, A. J. Spakowitz and J. A. Theriot, Bacterial chromosomal loci move subdiffusively through a viscoelastic cytoplasm, *Phys. Rev. Lett.*, 2010, **104**, 238102.
- 116 S. C. Weber, J. A. Theriot and A. J. Spakowitz, Subdiffusive motion of a polymer composed of subdiffusive monomers, *Phys. Rev. E*, 2010, **82**, 011913.
- 117 A. Javer, N. J. Kuwada, Z. Long, V. G. Benza, K. D. Dorfman, P. A. Wiggins, P. Cicuta and M. C. Lagomarsino, Persistent super-diffusive motion of *Escherichia coli* chromosomal loci, *Nat. Commun.*, 2014, **5**, 3854.
- 118 L. Stadler and M. Weiss, Non-equilibrium forces drive the anomalous diffusion of telomeres in the nucleus of mammalian cells, *New J. Phys.*, 2017, **19**, 113048.
- 119 A. E. Hafner, L. Santen, H. Rieger and M. R. Shaebani, Run-and-pause dynamics of cytoskeletal motor proteins, *Sci. Rep.*, 2016, **6**, 37162.
- 120 F. Pinaud, S. Clarke, A. Sittner and M. Dahan, Probing cellular events, one quantum dot at a time, *Nat. Methods*, 2010, **7**, 275.
- 121 A. Dreher, I. S. Aranson and K. Kruse, Spiral actin-polymerisation waves can generate amoeboidal cell crawling, *New J. Phys.*, 2014, **16**, 055007.
- 122 R. Shlomovitz and N. S. Gov, Membrane waves driven by actin and myosin, *Phys. Rev. Lett.*, 2007, **98**, 168103.
- 123 K. Doubrovinski and K. Kruse, Cell motility resulting from spontaneous polymerisation waves, *Phys. Rev. Lett.*, 2011, **107**, 258103.
- 124 F. Peruani and L. G. Morelli, Self-propelled particles with fluctuating speed and direction of motion in two dimensions, *Phys. Rev. Lett.*, 2007, **99**, 010602.
- 125 O. Chepizhko and F. Peruani, Diffusion, subdiffusion, and trapping of active particles in heterogeneous media, *Phys. Rev. Lett.*, 2013, **111**, 160604.
- 126 O. Chepizhko and F. Peruani, Active particles in heterogeneous media display new physics, *Eur. Phys. J.: Spec. Top.*, 2015, **224**, 1287.
- 127 F. Detcheverry, Generalized run-and-turn motions: From bacteria to Lévy walks, *Phys. Rev. E*, 2017, **96**, 012415.
- 128 C. A. Condat and G. J. Sibona, Diffusion in a model for active Brownian motion, *Phys. D*, 2002, **168–169**, 235.
- 129 D. Selmecki, S. F. Tolic-Nørrelykke, E. Schaffer, P. H. Hagedorn, S. Mosler, K. Berg-Sorensen, N. B. Larsen and H. Flyvbjerg, Brownian motion after Einstein and Smoluchowski: Some new applications and new experiments, *Acta Phys. Pol., B*, 2007, **38**, 2407.
- 130 M. Schienbein and H. Gruler, Langevin equation, Fokker-Planck equation and cell migration, *Bull. Math. Biol.*, 1993, **55**, 585.
- 131 P. Romanczuk and L. Schimansky-Geier, Brownian motion with active fluctuations, *Phys. Rev. Lett.*, 2011, **106**, 230601.
- 132 C. L. Vestergaard, J. N. Pedersen, K. I. Mortensen and H. Flyvbjerg, Estimation of motility parameters from trajectory data, *Eur. Phys. J.: Spec. Top.*, 2015, **224**, 1151.
- 133 J. N. Pedersen, L. Li, C. Gradinaru, R. H. Austin, E. C. Cox and H. Flyvbjerg, How to connect time-lapse recorded trajectories of motile microorganisms with dynamical models in continuous time, *Phys. Rev. E*, 2016, **94**, 062401.
- 134 K. Kroy and F. Cichos, Hot Brownian Motion, in *Diffusive Spreading in Nature, Technology and Society*, ed. A. Bunde, J. Caro, J. Kärgler, and G. Vogl, Springer, 2018.
- 135 E. Kepten, A. Weron, G. Sikora, K. Burnecki and Y. Garini, Guidelines for the fitting of anomalous diffusion mean square displacement graphs from single particle tracking experiments, *PLoS One*, 2015, **10**, e0117722.

- 136 A. G. Cherstvy, A. V. Chechkin and R. Metzler, Anomalous diffusion and ergodicity breaking in heterogeneous diffusion processes, *New J. Phys.*, 2013, **15**, 083039.
- 137 A. G. Cherstvy and R. Metzler, Nonergodicity, fluctuations, and criticality in heterogeneous diffusion processes, *Phys. Rev. E*, 2014, **90**, 012134.
- 138 A. G. Cherstvy, A. V. Chechkin and R. Metzler, Ageing and confinement in non-ergodic heterogeneous diffusion processes, *J. Phys. A: Math. Theor.*, 2014, **47**, 485002.
- 139 A. G. Cherstvy and R. Metzler, Ergodicity breaking, ageing, and confinement in generalized diffusion processes with position and time dependent diffusivity, *J. Stat. Mech.: Theory Exp.*, 2015, **P05010**, 1–20.
- 140 J. Saragosti, P. Silberzan and A. Buguin, Modeling *E. coli* tumbles by rotational diffusion. Implications for chemotaxis, *PLoS One*, 2012, **7**, e35412.
- 141 J. L. Lebowitz and O. Penrose, Modern ergodic theory, *Phys. Today*, 1973, **26**(2), 23.
- 142 J.-P. Bouchaud, Weak ergodicity breaking and aging in disordered systems, *J. Phys. I*, 1992, **2**, 1705.
- 143 G. Bel and E. Barkai, Weak ergodicity breaking in the continuous-time random walk, *Phys. Rev. Lett.*, 2005, **94**, 240602.
- 144 A. Rebenshtok and E. Barkai, Distribution of time-averaged observables for weak ergodicity breaking, *Phys. Rev. Lett.*, 2007, **99**, 210601.
- 145 M. T. Valentine, P. D. Kaplan, D. Thota, J. C. Crocker, T. Gisler, R. K. Prud'homme, M. Beck and D. A. Weitz, Investigating the microenvironments of inhomogeneous soft materials with multiple particle tracking, *Phys. Rev. E*, 2001, **64**, 061506.
- 146 T. Wagner, A. Kroll, C. R. Haramagatti, H.-G. Lipinski and M. Wiemann, Classification and segmentation of nanoparticle diffusion trajectories in cellular micro environments, *PLoS One*, 2017, **12**, e0170165.
- 147 C. E. Wagner, "Micro- and macro-rheological studies of the structure and association dynamics of biopolymer gels", PhD thesis, Massachusetts Institute of Technology, 2018.
- 148 S. Cornillon, R. Froquet and P. Cosson, Involvement of Sib proteins in the regulation of cellular adhesion in *Dictyostelium discoideum*, *Eukaryotic Cell*, 2008, **7**, 1600.
- 149 K. Burnecki, E. Kepten, Y. Garini, G. Sikora and A. Weron, Estimating the anomalous diffusion exponent for single particle tracking data with measurement errors – An alternative approach, *Sci. Rep.*, 2015, **5**, 11306.
- 150 C. L. Vestergaard, P. C. Blainey and H. Flyvbjerg, Optimal estimation of diffusion coefficients from single-particle trajectories, *Phys. Rev. E*, 2014, **89**, 022726.
- 151 K. Burnecki, E. Kepten, J. Janczura, I. Bronshtein, Y. Garini and A. Weron, Universal algorithm for identification of fractional Brownian motion. A case of telomere subdiffusion, *Biophys. J.*, 2012, **103**, 1839.
- 152 X. Michalet, Mean square displacement analysis of single-particle trajectories with localization error: Brownian motion in an isotropic medium, *Phys. Rev. E*, 2010, **82**, 041914.
- 153 J. S. Crater and R. L. Carrier, Barrier properties of gastrointestinal mucus to nanoparticle transport, *Macromol. Biosci.*, 2010, **10**, 1473.
- 154 N. Makarava, S. Benmehdi and M. Holschneider, Bayesian estimation of self-similarity exponent, *Phys. Rev. E*, 2011, **84**, 021109.
- 155 F. Etoc, E. Balloul, C. Vicario, D. Normanno, D. Liße, A. Sittner, J. Piehler, M. Dahan and M. Coppey, Non-specific interactions govern cytosolic diffusion of nanosized objects in mammalian cells, *Nat. Mater.*, 2018, **17**, 740.
- 156 K. Speckner, L. Stadler and M. Weiss, Anomalous dynamics of the endoplasmic reticulum network, *Phys. Rev. E*, 2018, **98**, 012406.
- 157 M. J. Saxton, Single-particle tracking: the distribution of diffusion coefficients, *Biophys. J.*, 1997, **72**, 1744.
- 158 A. G. Cherstvy, S. Thapa, C. E. Wagner and R. Metzler, Non-Gaussian, non-ergodic, and non-Fickian diffusion in mucin hydrogels, 2018, work in preparation.
- 159 T. J. Lampo, S. Stylianidou, M. P. Backlund, P. A. Wiggins and A. J. Spakowitz, Cytoplasmic RNA-protein particles exhibit non-Gaussian subdiffusive behavior, *Biophys. J.*, 2017, **112**, 1.
- 160 B. Wang, S. M. Anthony, S. C. Bae and S. Granick, Anomalous yet Brownian, *Proc. Natl. Acad. Sci. U. S. A.*, 2009, **106**, 15160.
- 161 B. Wang, J. Kuo, S. C. Bae and S. Granick, When Brownian diffusion is not Gaussian, *Nat. Mater.*, 2012, **11**, 481.
- 162 S. Hapca, J. W. Crawford and I. M. Young, Anomalous diffusion of heterogeneous populations characterized by normal diffusion at the individual level, *J. R. Soc., Interface*, 2009, **6**, 111.
- 163 M. V. Chubynsky and G. W. Slater, Diffusing diffusivity: a model for anomalous, yet Brownian, diffusion, *Phys. Rev. Lett.*, 2014, **113**, 098302.
- 164 A. V. Chechkin, F. Seno, R. Metzler and I. M. Sokolov, Brownian yet non-Gaussian diffusion: from superstatistics to subordination of diffusing diffusivities, *Phys. Rev. X*, 2017, **7**, 021002.
- 165 R. Metzler, Gaussianity fair: the riddle of anomalous yet non-Gaussian diffusion, *Biophys. J.*, 2017, **112**, 413.
- 166 J. Slezak, R. Metzler and M. Magdziarz, Superstatistical generalised Langevin equation: non-Gaussian viscoelastic anomalous diffusion, *New J. Phys.*, 2018, **20**, 023026.
- 167 C. Beck and E. G. D. Cohen, Superstatistics, *Phys. A*, 2003, **322**, 267.
- 168 H. U. Bödeker, C. Beta, T. D. Frank and E. Bodenschatz, Quantitative analysis of random ameboid motion, *Europhys. Lett.*, 2010, **90**, 28005.
- 169 S. Vedel, S. Tayb, D. M. Johnston, H. Bruus and S. R. Quake, Migration of cells in a social context, *Proc. Natl. Acad. Sci. U. S. A.*, 2013, **110**, 129.
- 170 D. Selmecki, S. Mosler, P. H. Hagedorn, N. B. Larsen and H. Flyvbjerg, Cell motility as persistent random motion: theories from experiments, *Biophys. J.*, 2005, **89**, 912.
- 171 C. P. McCann, E. C. Rericha, C. Wang, W. Losert and C. A. Parent, *Dictyostelium* cells migrate similarly on

- surfaces of varying chemical composition, *PLoS One*, 2014, **9**, e87981.
- 172 [http://dictybase.org/strain\\_history.htm](http://dictybase.org/strain_history.htm).
- 173 H. C. Berg, *E. coli* in Motion, Springer, 2004.
- 174 M. Schwarzl, A. Godec and R. Metzler, Quantifying non-ergodicity of anomalous diffusion with higher order moments, *Sci. Rep.*, 2017, **7**, 3878.
- 175 M. Magdziarz, A. Weron, K. Burnecki and J. Klafter, Fractional Brownian motion versus the continuous-time random walk: a simple test for subdiffusive dynamics, *Phys. Rev. Lett.*, 2009, **103**, 180602.
- 176 G. Sikora, M. Teuerle, A. Wylomanska and D. Grebenkov, Statistical properties of the anomalous scaling exponent estimator based on time-averaged mean-square displacement, *Phys. Rev. E*, 2017, **96**, 022132.
- 177 V. Tejedor, O. Benichou, R. Voituriez, R. Jungmann, F. Simmel, C. Selhuber-Unkel, L. B. Oddershede and R. Metzler, Quantitative analysis of single particle trajectories: mean maximal excursion method, *Biophys. J.*, 2010, **98**, 1364.
- 178 D. Ernst, J. Köhler and M. Weiss, Probing the type of anomalous diffusion with single-particle tracking, *Phys. Chem. Chem. Phys.*, 2014, **16**, 7686.
- 179 M. F. Serag and S. Habuchi, Conserved linear dynamics of single-molecule Brownian motion, *Nat. Commun.*, 2017, **8**, 15675.
- 180 G. Sikora, E. Kepten, A. Weron, M. Balcerek and K. Burnecki, An efficient algorithm for extracting the magnitude of the measurement error for fractional dynamics, *Phys. Chem. Chem. Phys.*, 2017, **19**, 26566.
- 181 V. Briane, C. Kervrann and M. Vimondz, A statistical analysis of particle trajectories in living cells, *Phys. Rev. E*, 2018, **97**, 062121.
- 182 S. Thapa, M. A. Lomholt, J. Krog, A. G. Cherstvy and R. Metzler, Bayesian nested-sampling analysis of single-particle tracking data, *Phys. Chem. Chem. Phys.*, 2018, submitted.
- 183 F. Thiel and I. M. Sokolov, Weak ergodicity breaking in an anomalous diffusion process of mixed origins, *Phys. Rev. E*, 2014, **89**, 012136.
- 184 H. Qian, M. P. Sheetz and E. L. Elson, Single particle tracking: analysis of diffusion and flow in two-dimensional systems, *Biophys. J.*, 1991, **60**, 910.
- 185 E. A. Codling, M. J. Plank and S. Benhamou, Random walk models in biology, *J. R. Soc., Interface*, 2008, **5**, 813.
- 186 M. Lysy, N. S. Pillai, D. B. Hill, M. G. Forest, J. Mellnik, P. Vasquez and S. A. McKinley, Model comparison and assessment for single particle tracking in biological fluids, *J. Am. Stat. Assoc.*, 2016, **111**, 1413.
- 187 F. Thiel and I. M. Sokolov, Scaled Brownian motion as a mean-field model for continuous-time random walks, *Phys. Rev. E*, 2014, **89**, 012115.
- 188 Y. Meroz, I. M. Sokolov and J. Klafter, Test for determining a subdiffusive model in ergodic systems from single trajectories, *Phys. Rev. Lett.*, 2013, **110**, 090601.
- 189 F. Thiel, F. Flegel and I. M. Sokolov, Disentangling sources of anomalous diffusion, *Phys. Rev. Lett.*, 2013, **111**, 010601.
- 190 I. H. Riedel, K. Kruse and J. Howard, A self-organized vortex array of hydrodynamically entrained sperm cells, *Science*, 2005, **309**, 300.
- 191 A. Martín-Gomez, D. Levis, A. Díaz-Guilera and I. Pagonabarraga, Collective motion of active Brownian particles with polar alignment, *Soft Matter*, 2018, **14**, 2610.
- 192 W. Ponisch and V. Zaburdaev, Relative distance between tracers as a measure of diffusivity within moving aggregates, *Eur. Phys. J. B*, 2018, **91**, 27.
- 193 J. C. Crocker, M. T. Valentine, E. R. Weeks, T. Gisler, P. D. Kaplan, A. G. Yodh and D. A. Weitz, Two-point microrheology of inhomogeneous soft materials, *Phys. Rev. Lett.*, 2000, **85**, 888.
- 194 T. Neusius, I. M. Sokolov and J. C. Smith, Subdiffusion in time-averaged, confined random walks, *Phys. Rev. E*, 2009, **80**, 011109.
- 195 F. Thiel and I. M. Sokolov, Time averages in continuous-time random walks, *Phys. Rev. E*, 2017, **95**, 022108.
- 196 A. G. Cherstvy and R. Metzler, Population splitting, trapping, and non-ergodicity in heterogeneous diffusion processes, *Phys. Chem. Chem. Phys.*, 2013, **15**, 20220.
- 197 J. H. P. Schulz, E. Barkai and R. Metzler, Aging effects and population splitting in single-particle trajectory averages, *Phys. Rev. Lett.*, 2013, **110**, 020602.
- 198 J. H. P. Schulz, E. Barkai and R. Metzler, Aging renewal theory and application to random walks, *Phys. Rev. X*, 2014, **4**, 011028.
- 199 S. Petrovskii, A. Mashanova and V. A. A. Jansen, Variation in individual walking behavior creates the impression of a Lévy flight, *Proc. Natl. Acad. Sci. U. S. A.*, 2011, **108**, 8704.
- 200 S. Pigolotti and R. Benzi, Competition between fast- and slow-diffusing species in non-homogeneous environments, *J. Theor. Biol.*, 2016, **395**, 204.
- 201 S. Sadegh, J. L. Higgins, P. C. Mannion, M. M. Tamkun and D. Krapf, Plasma membrane is compartmentalized by a self-similar cortical actin meshwork, *Phys. Rev. X*, 2017, **7**, 011031.
- 202 J. Guan, B. Wang and S. Granick, Even hard-sphere colloidal suspensions display Fickian yet non-Gaussian diffusion, *ACS Nano*, 2014, **8**, 3331.
- 203 C. Manzo, J. A. Torreno-Pina, P. Massignan, G. J. Lapeyre, Jr., M. Lewenstein and M. F. Garcia Parajo, Weak ergodicity breaking of receptor motion in living cells stemming from random diffusivity, *Phys. Rev. X*, 2015, **5**, 011021.
- 204 G. Kwon, B. J. Sung and A. Yethiraj, Dynamics in crowded environments: is non-Gaussian Brownian diffusion normal?, *J. Phys. Chem. B*, 2014, **118**, 8128.
- 205 D. Wang, C. He, M. P. Stoykovich and D. K. Schwartz, Nanoscale topography influences polymer surface diffusion, *ACS Nano*, 2015, **9**, 1656.
- 206 T. Toyota, D. A. Head, C. F. Schmidt and D. Mizuno, Non-Gaussian athermal fluctuations in active gels, *Soft Matter*, 2011, **7**, 3234.
- 207 F. Babayekhorasani, D. E. Dunstan, R. Krishnamoorti and J. C. Conrad, Nanoparticle diffusion in crowded and confined media, *Soft Matter*, 2016, **12**, 8407.

- 208 C. Xue, X. Zheng, K. Chen, Y. Tian and G. Hu, Probing non-Gaussianity in confined diffusion of nanoparticles, *J. Phys. Chem. Lett.*, 2016, **7**, 514.
- 209 C. Metzner, C. Mark, J. Steinwachs, L. Lautscham, F. Stadler and B. Fabry, Superstatistical analysis and modelling of heterogeneous random walks, *Nat. Commun.*, 2015, **6**, 7516.
- 210 D. S. Banks, C. Tressler, R. D. Peters, F. Höfling and C. Fradin, Characterizing anomalous diffusion in crowded polymer solutions and gels over five decades in time with variable-lengthscale fluorescence correlation spectroscopy, *Soft Matter*, 2016, **12**, 4190.
- 211 K. He, F. B. Khorasani, S. T. Retterer, D. K. Thomas, J. C. Conrad and R. Krishnamoort, Diffusive dynamics of nanoparticles in arrays of nanoposts, *ACS Nano*, 2013, **7**, 5122.
- 212 G. Campagnola, K. Nepal, B. W. Schroder, O. B. Peersen and D. Krapf, Superdiffusive motion of membrane-targeting C2 domains, *Sci. Rep.*, 2015, **5**, 17721.
- 213 D. Krapf, Mechanisms underlying anomalous diffusion in the plasma membrane, *Curr. Top. Membr.*, 2015, **75**, 167.
- 214 C. E. Wagner, B. S. Turner, M. Rubinstein, G. H. McKinley and K. Ribbeck, A rheological study of the association and dynamics of MUC5AC gels, *Biomacromolecules*, 2017, **18**, 3654.
- 215 W. He, H. Song, Y. Su, L. Geng, B. J. Ackerson, H. B. Peng and P. Tong, Dynamic heterogeneity and non-Gaussian statistics for acetylcholine receptors on live cell membrane, *Nat. Commun.*, 2016, **7**, 11701.
- 216 M. J. Skaug, J. Mabry and D. K. Schwartz, Intermittent molecular hopping at the solid-liquid interface, *Phys. Rev. Lett.*, 2013, **110**, 256101.
- 217 B. Stuhmann, M. S. Silva, M. Depken, F. C. MacKintosh and G. H. Koenderink, Nonequilibrium fluctuations of a remodeling *in vitro* cytoskeleton, *Phys. Rev. E*, 2012, **86**, 020901(R).
- 218 M. J. Skaug, J. N. Mabry and D. K. Schwartz, Single-molecule tracking of polymer surface diffusion, *J. Am. Chem. Soc.*, 2014, **136**, 1327.
- 219 M. J. Skaug and D. K. Schwartz, Tracking nanoparticle diffusion in porous filtration media, *Ind. Eng. Chem. Res.*, 2015, **54**, 4414.
- 220 D. Wang, R. Hu, M. J. Skaug and D. K. Schwartz, Temporally anti-correlated motion of nanoparticles at a liquid interface, *J. Phys. Chem. Lett.*, 2015, **6**, 54.
- 221 B. R. Parry, I. V. Surovtsev, M. T. Cabeen, C. S. O'Hern, E. R. Dufresne and C. Jacobs-Wagner, The bacterial cytoplasm has glass-like properties and is fluidized by metabolic activity, *Cell*, 2014, **156**, 183.
- 222 R. Jain and K. L. Sebastian, Diffusion in a crowded, rearranging environment, *J. Phys. Chem. B*, 2016, **120**, 3988.
- 223 R. Jain and K. L. Sebastian, Lévy flight with absorption: a model for diffusing diffusivity with long tails, *Phys. Rev. E*, 2017, **95**, 032135.
- 224 P. Massignan, C. Manzo, J. A. Torreno-Pina, M. F. Garcia-Parajo, M. Lewenstein and G. J. Lapeyre, Jr., Nonergodic subdiffusion from Brownian motion in an inhomogeneous medium, *Phys. Rev. Lett.*, 2014, **112**, 150603.
- 225 T. Miyaguchi, T. Akimoto and E. Yamamoto, Langevin equation with fluctuating diffusivity: a two-state model, *Phys. Rev. E*, 2016, **94**, 012109.
- 226 T. Akimoto and E. Yamamoto, Distributional behavior of diffusion coefficients obtained by single trajectories in annealed transit time model, *J. Stat. Mech.: Theory Exp.*, 2016, 123201.
- 227 A. G. Cherstvy and R. Metzler, Anomalous diffusion in time-fluctuating non-stationary diffusivity landscapes, *Phys. Chem. Chem. Phys.*, 2016, **18**, 23840.
- 228 T. Akimoto and E. Yamamoto, Distributional behaviors of time-averaged observables in the Langevin equation with fluctuating diffusivity: normal diffusion but anomalous fluctuations, *Phys. Rev. E*, 2016, **93**, 062109.
- 229 D. Michieletto, N. Nahali and A. Rosa, Glassiness and heterogeneous dynamics in dense solutions of ring polymers, *Phys. Rev. Lett.*, 2017, **119**, 197801.
- 230 J. Kim, C. Kim and B. J. Sung, Simulation study of seemingly Fickian but heterogeneous dynamics of two dimensional colloids, *Phys. Rev. Lett.*, 2013, **110**, 047801.
- 231 E. Yamamoto, A. C. Kalli, T. Akimoto, K. Yasuoka and M. S. P. Sansom, Anomalous dynamics of a lipid recognition protein on a membrane surface, *Sci. Rep.*, 2015, **5**, 18245.
- 232 C. Chipot and J. Comer, Subdiffusion in membrane permeation of small molecules, *Sci. Rep.*, 2016, **6**, 35913.
- 233 S. K. Ghosh, A. G. Cherstvy and R. Metzler, Non-universal tracer diffusion in crowded media of non-inert obstacles, *Phys. Chem. Chem. Phys.*, 2015, **17**, 1847.
- 234 E. Yamamoto, T. Akimoto, A. C. Kalli, K. Yasuoka and M. S. P. Sansom, Dynamic interactions between a membrane binding protein and lipids induce fluctuating diffusivity, *Sci. Adv.*, 2017, **3**, e1601871.
- 235 E. Yamamoto, T. Akimoto, M. Yasui and K. Yasuoka, Origin of subdiffusion of water molecules on cell membrane surfaces, *Sci. Rep.*, 2014, **4**, 4720.
- 236 T. Akimoto, E. Yamamoto, K. Yasuoka, Y. Hirano and M. Yasui, Non-gaussian fluctuations resulting from power-law trapping in a lipid bilayer, *Phys. Rev. Lett.*, 2011, **107**, 178103.
- 237 A. V. Weigel, B. Simon, M. M. Tamkun and D. Krapf, Ergodic and nonergodic processes coexist in the plasma membrane as observed by single-molecule tracking, *Proc. Natl. Acad. Sci. U. S. A.*, 2011, **108**, 6438.
- 238 R. Friedrich, J. Peinke, M. Sahimi and M. R. R. Tabar, Approaching complexity by stochastic methods: from biological systems to turbulence, *Phys. Rep.*, 2011, **506**, 87.
- 239 J. C. Crocker and D. G. Grier, Methods of digital video microscopy for colloidal studies, *J. Colloid Interface Sci.*, 1996, **179**, 298.
- 240 M. Theves, *Bacterial motility and growth in open and confined environments*, PhD thesis, University of Potsdam, 2013.
- 241 J. Tailleur and M. E. Cates, Statistical mechanics of interacting run-and-tumble bacteria, *Phys. Rev. Lett.*, 2008, **100**, 218103.
- 242 M. H. G. Duits, Y. Li, S. A. Vanapalli and F. Mugele, Mapping of spatiotemporal heterogeneous particle dynamics in living cells, *Phys. Rev. E*, 2009, **79**, 051910.

- 243 The vegetative DICTY cells diffuse significantly faster at low densities<sup>47</sup> (up to 5 times faster as the cell density  $\rho$  decreases from  $3 \times 10^4$  to just 50 cells per  $\text{cm}^2$ ), and the amount of quorum-sensing factors governs the motility.<sup>47</sup> Moreover, there exists a critical cell-to-cell distance of  $\sim 100 \mu\text{m}$  (or  $\sim 10^4$  cells per  $\text{cm}^2$ ) below which the cells (the DH1 strain) can measurably sense one another.<sup>47</sup> Additionally, the effects of ageing in the DICTY dynamics are also important, with the diffusion coefficient dropping within 12 hours for a cell density of  $\rho \approx 10^4$  cells per  $\text{cm}^2$  from  $\sim 8$  to  $\sim 3 \mu\text{m}^2 \text{min}^{-1}$ , see Fig. 3A and B in ref. 47. Moreover, ageing effects depend on the medium conditions and additional flows.<sup>47</sup> Recently, the effects of ageing and stress on the motility of superdiffusive nematode worms *Caenorhabditis elegans* were studied<sup>85</sup>.
- 244 Superdiffusive motion of another free-living amoeba, *Acanthamoeba castellanii*, was studied in ref. 7. The relation of intracellular motions<sup>87</sup> and the effects of cytoskeletal elements on cell locomotion were established. The implications of treatments with blebbistatin (inhibiting myosin-II motors) and nocodazole (inducing microtubuli depolymerisation) were analysed, see also ref. 8. The motion of intra-amoeboid particles was found to stay superdiffusive after the inhibition of polymerisation of the cytoskeletal elements,<sup>7</sup> while the motion was almost localised when myosin motors were switched off<sup>7</sup>.
- 245 Note also that for human granulocytes<sup>130</sup> the MSD was also shown to grow with time as  $\langle \delta_{\text{WLC}}^2(A) \rangle$ , see also ref. 5, 32, 51, 95 and 129. This correlated motion at short times, interrupted by random changes in cell directions, is reminiscent of the run-and-tumble dynamics of *Escherichia coli*<sup>15,127,140</sup> and other bacteria<sup>16,27,241</sup>.
- 246 Persistent DICTY motion was previously characterised in ref. 75 based on the model of fractional Brownian motion, with the average Hurst exponent  $H = \alpha/2 \approx 0.6$ . A Bayesian estimation<sup>154</sup> of the self-similarity exponent was performed. For short trajectories the values of  $H$  were shown to vary from about 0.2 to 0.8,<sup>75</sup> with the distribution of  $H$  changing for short (50–150), intermediate (150–500), and long ( $> 500$  steps) traces (a time step of 2 s).<sup>75</sup> For longer DICTY tracks the motion was shown on average to be more persistent, with smaller fluctuations of  $H$  along the trajectory. To study the time dependence of  $H$ , a sliding-window approach was used. As compared to the Bayesian analysis,<sup>75</sup> we compute the exponents  $\beta_i$  from the short-lag-time slopes of the time-averaged MSD trajectories.
- 247 We mention that shorter cell trajectories in the analysed, data set—statistically attributable to faster and more persistent cells in the population—are severely over-represented, see Fig. 9. This fact—when ensemble averaging the recorded traces (5)—will result in a more superdiffusive behaviour of  $\langle \delta^2(A) \rangle$  in the region of short lag times. To avoid a bias emerging from a non-uniform distribution of  $p(T)$ , the proportion of trajectories of all lengths should (ideally) be kept the same in the experiments (see also the discussion in ref. 155). This was not enforced for the current data set, certainly affecting the results of the analysis, in particular regarding the magnitude and scaling exponent of ensemble-averaged  $\delta^2$  in the region of intermediate and long lag times, as compared to the results of Fig. 2. Evidently, the non-Gaussian features of cell-displacement distributions, see Fig. 5 below, may also be somewhat affected by these details of data acquisition.
- 248 Note also here that ensemble averaging of time-averaged trajectories, eqn (5), clearly smears out some diffusive features, such as trajectory-to-trajectory variation. A more statistically-insightful way could be to divide the whole set of  $\{\delta^2(A)\}$  into subpopulations of most superdiffusive and strongly confined trajectories, as well as subsets in between, see ref. 145–147, and then perform averaging among these subsets separately. To do so and to extract statistically-meaningful results, the data set should be much larger than the current one, for which we performed no data pre-treatment (e.g., removal of a fraction of confined/stalling as well as of the fastest trajectories).
- 249 This is smaller than  $\langle v \rangle \approx 5.6 \mu\text{m min}^{-1}$  reported for non-chemotactic cells of the AX3 strain after 4–6 hours into the development cycle in ref. 66,  $\langle v \rangle \approx 4.3 \mu\text{m min}^{-1}$  estimated for heterogeneous populations of vegetative DICTY cells of the DH1 strain in ref. 47,  $\langle v \rangle \approx 7 \mu\text{m min}^{-1}$  for freely-diffusing AX4 strain cells in ref. 19,  $\langle v \rangle \approx 7.2 \mu\text{m min}^{-1}$  for pre-aggregative cells of the NC4 DICTY strain in ref. 46, and  $\langle v \rangle \approx 8 \mu\text{m min}^{-1}$  for chemotactically-active wild-type cells of the AX3 strain in ref. 53. This discrepancy can have multiple reasons: different DICTY strains used in experiments, variable cell–substrate adhesion properties,<sup>171</sup> different buffer compositions or diffusion media, and variable cell densities. Note that the cell shape also strongly affects its motile properties, with more elongated cells moving on average considerably faster than “round” and “split” ones (see Fig. 3D in ref. 56 for the AX2 DICTY strain). The minimal speed for a motile DICTY sub-population was set in ref. 56 to  $\langle v \rangle \approx 2.4 \mu\text{m min}^{-1}$ , close to the average speed we observed for the same AX2 strain. The reader is referred here to Table 6 of ref. 46 summarising the dramatic discrepancy in the values of average speeds, diffusion coefficients, and persistence times for different DICTY strains and mutants, including NC4, P2, N15F, and AX3 (see also ref. 172 for the history of strains). The variations of motility for vegetative cells of DH1-10 DICTY cells were analysed before,<sup>148</sup> including the effects of cell density (the DH1 strain)<sup>47</sup>.
- 250 Let us also mention some aspects of the data-acquisition frequency for tracking DICTY cells. In ref. 51 the time step was  $\delta t = 5$  s, with a data recording time of  $\sim 11$ –23 hours. In ref. 19 the time step was  $\delta t = 10$  s, with an overall tracking time of  $\approx 8$ –10 hours (compare to  $\delta t = 1/3$  min used here), see also ref. 168. Thus, the DICTY dynamics at very short times cannot be accessed in our statistical analysis and the features of repetitive run-and-turn dynamics (expected for these cells) may be smeared out. Based on the average speed of DICTY cells we monitored, their Reynolds number is  $\text{Re} \sim 10^{-6}$  (for comparison,  $\text{Re} \sim 10^{-5}$  for a full-speed swimming *Escherichia coli*<sup>173</sup>), while the Péclet number is  $\text{Pe} \sim 10$ .